Estimates of atmospheric-processed soluble iron from observations and a global mineral aerosol model: Biogeochemical implications

J. L. Hand,[1,2] N. M. Mahowald,[1,3] Y. Chen,[4] R. L. Siefert,[4] C. Luo,[3] A. Subramaniam,[5] and I. Fung[6]

Received 26 January 2004; revised 7 May 2004; accepted 28 June 2004; published 8 September 2004.

[1] Desert dust deposition to the ocean may be a significant source of biogeochemically important elements, specifically iron. The bioavailability of iron in the oceans requires it to be in a soluble form, and because atmospheric iron in desert dust is typically insoluble, understanding the atmospheric processes that convert insoluble iron to more soluble forms is essential. Understanding these relationships is especially important in remote ocean regions where iron may be the limiting nutrient. Observations of soluble iron from 2001 cruise-based aerosol measurements over the Atlantic and Pacific Oceans ranged from 0 to 45% (mean of 4 ± 9%) in the fine mode (<2.5 μm in diameter) and 0 to 87% (mean of 2 ± 10%) in the coarse mode. We test two simple hypotheses of soluble iron enhancement in the atmosphere using a global model of mineral aerosols. The first method assumes that iron solubility increases as iron is exposed to solar radiation, approximating photoreduction reactions that are important pathways for enhancement of soluble iron in the presence of acidic solutions. The second process imitates cloud processing of iron by increasing the amount of soluble iron when the mineral aerosol comes into contact with a cloud. Both methods resulted in similar average magnitudes of percent soluble iron compared to observations but did not capture specific events or have sufficient variability, perhaps because the model does not include aerosol interactions between species other than mineral dust or other processes that may be important. *INDEX TERMS:* 0305 Atmospheric Composition and Structure: Aerosols and particles (0345, 4801); 0315 Atmospheric Composition and Structure: Biosphere/atmosphere interactions; 0312 Atmospheric Composition and Structure: Air/sea constituent fluxes (3339, 4504); 0330 Atmospheric Composition and Structure: Geochemical cycles; *KEYWORDS:* mineral aerosols, desert dust, soluble iron

Citation: Hand, J. L., N. M. Mahowald, Y. Chen, R. L. Siefert, C. Luo, A. Subramaniam, and I. Fung (2004), Estimates of atmospheric-processed soluble iron from observations and a global mineral aerosol model: Biogeochemical implications, *J. Geophys. Res.*, *109*, D17205, doi:10.1029/2004JD004574.

1. Introduction

[2] Iron is critical to ocean primary productivity because of its role as a rate-limiting nutrient for microorganisms. Iron has been hypothesized to limit phytoplankton productivity in high nitrate low-chlorophyll (HNLC) ocean regions [*Martin et al.*, 1991]. In these regions, chlorophyll levels are lower than expected because low concentrations of iron restrict the growth of phytoplankton and limit primary production [*Martin et al.*, 1991]. Areas of the world's oceans that are considered HNLC include the subarctic and equatorial Pacific Ocean and the Southern Ocean; these regions are also in areas of low dust deposition [e.g., *Fung et al.*, 2000]. In these regions, upwelled iron may be insufficient for the usage of other nutrients, therefore an external source of iron is required in order to utilize these nutrients [e.g., *Martin et al.*, 1991; *Measures and Vink*, 1999, 2000; *Fung et al.*, 2000; *Vink and Measures*, 2001]. Deposition of iron to these regions also has important implications for the CO_2 budget, as increases in iron to the oceans may result in a decrease of CO_2 in the atmosphere on glacial timescales [e.g., *Watson et al.*, 1994; *Cooper et al.*, 1996; *Lefèvre and Watson*, 1999; *Watson and Lefèvre*, 1999]. It also has been proposed that iron in marine aerosols may affect the sulfur cycle through oxidation reactions [*Zhuang et al.*, 1992] and in turn the climate

[1]National Center for Atmospheric Research, Boulder, Colorado, USA.
[2]Now at Cooperative Institute for Research in the Atmosphere, Colorado State University, Fort Collins, Colorado, USA.
[3]Bren School of Environmental Science and Management and Institute for Computational Earth System Science, University of California, Santa Barbara, California, USA.
[4]Chesapeake Biological Laboratory, University of Maryland Center for Environmental Science, Solomons, Maryland, USA.
[5]Lamont-Doherty Earth Observatory of Columbia University, Palisades, New York, USA.
[6]Department of Earth and Planetary Science, University of California, Berkeley, California, USA.

0148-0227/04/2004JD004574

Table 1. Published Iron Solubility Values[a]

Location	Iron Solubility, %	Reference
North Pacific Ocean and Barbados	<1–49	*Zhuang et al.* [1990, 1992] and *Zhu et al.* [1993, 1997]
U.S. sites	<50	*Siefert et al.* [1997]
Arabian Sea	<4	*Siefert et al.* [1999]
North Atlantic Ocean	0.51	*Johansen et al.* [2000]
Antarctica	10–90	*Edwards and Sedwick* [2001]
Equatorial Atlantic Ocean	~2–7	*Chen and Siefert* [2003, 2004]
Equatorial Pacific Ocean	~1.7	*Chen and Siefert* [2003, 2004]

[a]Values for this study correspond to fine mode averages.

feedback loop through dimethyl sulfide (DMS) oxidation and cloud condensation nuclei formation [*Charlson et al.*, 1987; *Turner et al.*, 1996].

[3] The biogeochemical processes involving iron in the ocean are dependent on the solubility of iron, which is a strong function of the oxidation state of iron along with its mineralogy. On average, the crustal abundance of iron is ~3.5% [*Duce and Tindale*, 1991], and is primarily insoluble ferric iron (Fe(III)) in aluminosilicate form [*Zhu et al.*, 1997]. Iron solubility in soils is on average less than 0.1%, (at an extraction pH of 4.65) [*Fung et al.*, 2000], implying that atmospheric processing of mineral aerosols may be important for increasing iron availability. Photochemical processes reducing iron to a more soluble state (Fe(II)) have been the focus of several experimental studies [e.g., *Zuo and Hoigné*, 1992; *Pehkonen et al.*, 1993; *Siefert et al.*, 1994; *Zuo*, 1995; *Saydam and Senyuva*, 2002]. These studies have shown that aqueous complexes between Fe(III) and specific organic and inorganic ligands can play an important role in the photoreduction of Fe(III) to Fe(II) in cloud water or deliquesced aerosols. The steady state concentrations of Fe(II) are strongly dependent on the pH of solution and the available solar radiation [*Zuo and Hoigné*, 1992].

[4] Several in situ observations have measured the solubility of iron in mineral aerosols (see Table 1). For example, *Zhuang et al.* [1990, 1992] found that Fe(II), extracted at a pH of 3–8, ranged from 2.2 to 49% of iron in the North Pacific Ocean and Barbados. *Zhu et al.* [1993] found Fe(II) (pH = 1) to be <1% of total iron in Barbados. *Zhu et al.* [1997] later observed a significant diurnal pattern with daytime values of Fe(II) twice as high as nighttime; daytime values of Fe(II) were a mean of 1.6% of total iron. *Siefert et al.* [1997] measured Fe(II) in fog water and cloud water at U.S. sites and found that higher fractions of Fe(II) occurred during the day, with rarely more than 50% of total iron as Fe(II). Over the Arabian Sea, *Siefert et al.* [1999] determined that Fe(II) in the aerosol was never more than 4% of total iron and that 80% of Fe(II) existed in the fine mode (<3 μm in diameter). In the North Atlantic, *Johansen et al.* [2000] observed the mean total Fe(II) to be 0.51% of total iron, with 86% of Fe(II) in the fine mode. *Edwards and Sedwick* [2001] measured values ranging from 10 to 90% from snow samples in Antarctica (20–2950 pg/g dissolvable iron). The range of observed values of Fe(II) from these various studies could be due to differences in measurement techniques and time from collection to analysis; however, atmospheric processes affecting these aerosols could play a large role, including cloud processing.

[5] The enhanced levels of Fe(II) in the fine mode as observed by *Siefert et al.* [1999] and *Johansen et al.* [2000] suggest that atmospheric transport may play a role in the size segregation of Fe(II), as large particles are selectively removed due to gravitational settling. However, different sources of iron may result in higher soluble fractions, as anthropogenic sources are more soluble than crustal sources, and are predominantly found in the fine mode [e.g., *Colin and Jaffrezo*, 1990; *Guieu et al.*, 1997]. Cloud processing of aerosols could also result in size dependence of soluble iron, as these processes are size and composition dependent. If processing is occurring only on the surface of aerosols, then we expect fine aerosols to be processed more quickly than coarse aerosols because of their higher surface to volume ratio. It is possible that enhanced solubility is due to variability in the iron sources, or may be occurring via transport and sequential cloud processing.

[6] For the first time we explore the relationship between soluble iron and the aerosol species that are thought to be active in enhancing iron solubility (non-sea-salt sulfate and organic acids). We use data from three different cruises in different ocean basins and seasons in order to gain insight into the processes that are thought to be important for soluble iron conversion. We also make the first attempt to explicitly model both iron content in mineral aerosols as well as percent iron solubility. We use an atmospheric transport model to investigate the roles of photoreduction reactions and cloud processing of mineral aerosols to enhance soluble iron in the atmosphere. Model estimates of soluble iron are compared with measurements of fine and coarse mode aerosol composition (including ionic and trace elemental species and oxidation states of iron) performed on board cruise ships as part of the MANTRA and PIRANA projects in the equatorial subtropical and tropical north Atlantic Oceans and Pacific Ocean in 2001. Understanding the processes and timescales for enhancing soluble iron is important for recognizing relationships that result in higher levels of bioavailable iron to the remote oceans, especially HNCL regions, or oligotrophic regions where nitrogen fixation provides a source of new nutrient nitrogen [*Capone*, 2001].

[7] This paper is organized in six sections. Section 2 describes measured total and soluble iron concentrations and other observed aerosol species. Section 3 includes a description of the 3-D transport model and the desert dust module used in this study. Model validation in the cruise-track regions with cruise-based measurements are in section 3.1, while validations with available satellite and surface-based measurements are presented in sections 3.2 and 3.3, respectively. Modeled soluble iron estimates and comparisons to observations are described in section 4. Implications for using global models for estimating iron solubility and deposition to world oceans will be discussed in section 5, and section 6 summarizes the study.

2. Cruise-Based Observations of Total and Soluble Iron

[8] The onboard cruise measurements were performed as part of the MANTRA and PIRANA projects in 2001 and described in detail by *Chen and Siefert* [2003, 2004]. These projects were designed to investigate oceanic nitro-

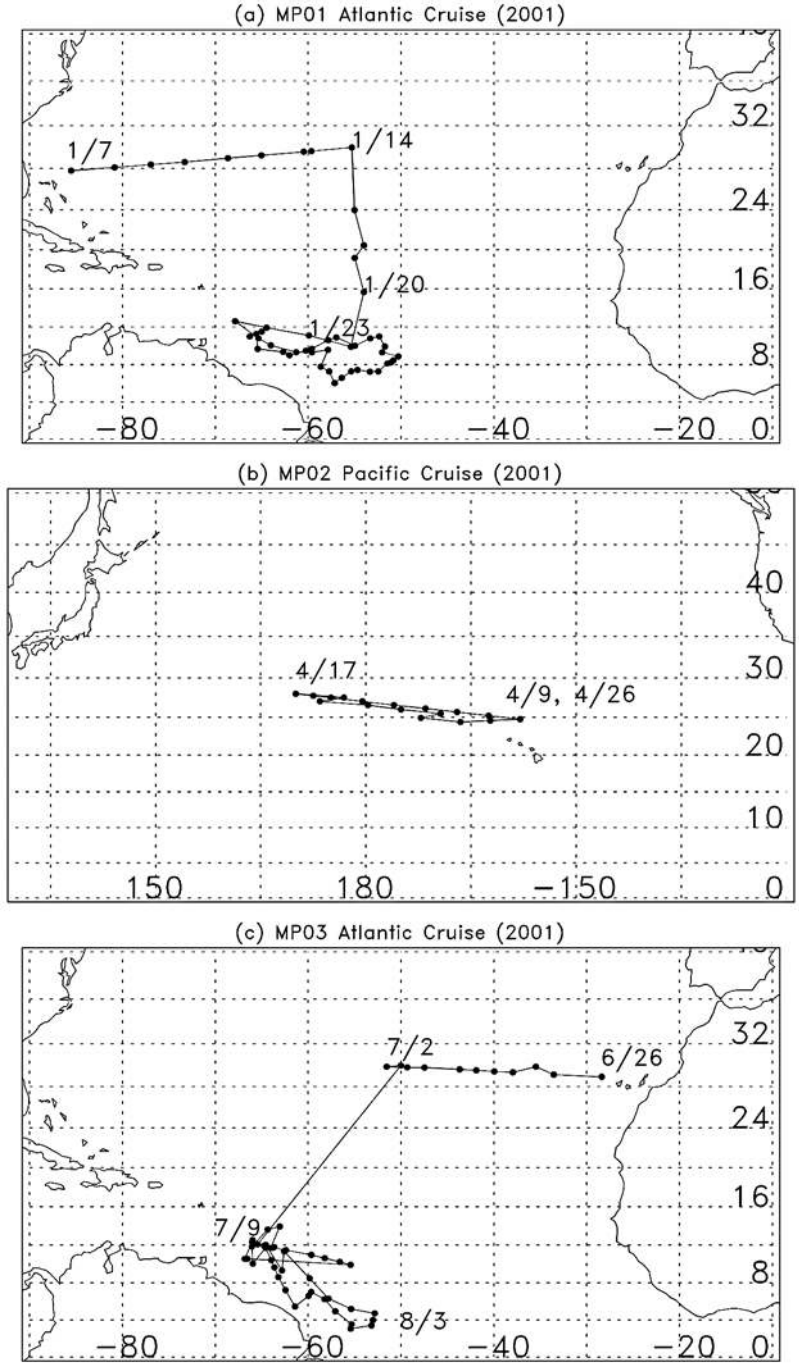

Figure 1. (a) Cruise track of MP01 (6 January to 22 February 2001). (b) Cruise track of MP02 (9–30 April 2001). (c) Cruise track of MP03 (25 June to 19 August 2001).

gen fixation and climate feedbacks (MANTRA) as well as plankton dynamics in the western equatorial Atlantic Ocean (PIRANA). Three cruises are evaluated in this paper. The first cruise (MP01) occurred on board the R/V *Seward Johnson* in the tropical Atlantic Ocean from 6 January to 22 February 2001. It began in Florida and then traveled south and sampled off the northern coast of South America for a total of 40 days (see Figure 1a). The second cruise (MP02) occurred on board the R/V *Wecoma* in the tropical Pacific Ocean from 9 to 30 April 2001. It traveled northwest from the coast of Hawaii before returning along the same track for a total of 21 days (see Figure 1b). The third cruise (MP03) occurred on board the R/V *Knorr* in the equatorial Atlantic Ocean from 25 June to 19 August 2001, leaving the Canary Islands and cruising west and then south, toward the northern coast of South America for a total of 50 days (see Figure 1c). The locations and time periods of these cruises reflect the typical patterns of long-range transport of Asian (Pacific) and African (Atlantic) dust due to seasonal changes in large-scale circulation patterns and the position of the Intertropical Convergence Zone [*Husar et al.*, 1997].

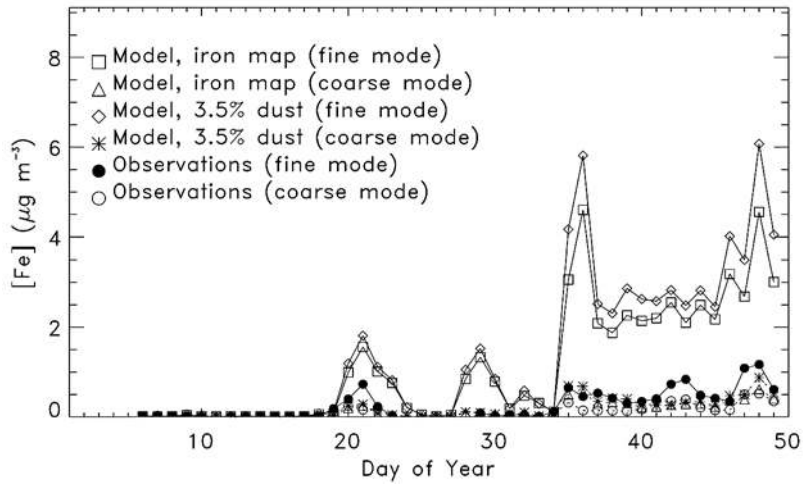

Figure 2. MP01 total iron concentrations (μg m^{-3}) from observations and two model estimates for the fine (diameter <2.5 μm) and coarse particle modes. Model estimates are derived from a dust source map (3.5% of dust is iron) and iron map.

[9] Aerosol measurements were performed on board using size resolved samplers to separate fine (diameter, D_p < 2.5 μm) and coarse mode (D_p > 2.5 μm) aerosol composition, following the methods outlined by *Chen and Siefert* [2003, 2004], *Siefert et al.* [1999] and *Johansen et al.* [1999, 2000]. Trace element concentrations were determined with an inductively coupled plasma-mass spectrometer (ICP-MS) and ion analyses were performed using ion chromatography (IC). Measurements of soluble Fe were conducted immediately after sample collection to reduce possible oxidation of Fe(II) to Fe(III) during storage. Total labile Fe measurements include the contributions of Fe(II) and Fe(III) that is easily reduced to Fe(II). Analytical procedures are described by *Chen and Siefert* [2003, 2004].

[10] We define iron solubility (Fe_{sol}) as the percent of total iron (Fe_{tot}) that is Fe(II) (e.g., Fe_{sol} = 100*Fe(II)/Fe_{tot}). Larger values of Fe_{sol} could be due to large concentrations of Fe(II), or small values of Fe_{tot}, or both. Values of Fe_{sol} that correspond to very low concentrations of Fe_{tot} may be subject to errors due to uncertainties in concentrations that are close to the detection limit. We use only Fe(II) (instead of Fe(II) and easily reducible Fe(III)) in the definition of Fe_{sol} because Fe(II) observations have been reported by other research groups and are less dependent on extraction methods.

2.1. Observed Total and Soluble Iron

[11] During MP01, the first Atlantic cruise (6 January to 22 February 2001), total iron was observed primarily in the fine mode (68%), and concentrations were relatively low during the first part of the cruise, and increased during the second part of the cruise, as the ship crossed into the main North African dust plume (see Figure 2). Table 2 lists the mean and one standard deviation in fine and coarse mode iron concentrations. Fine and coarse mode iron concentrations were highly correlated with aluminum (r = 0.99), suggesting that iron was associated with natural mineral aerosols. In all of the tables, the correlation coefficients statistically significant at a 95% level are bolded. These levels were computed with the effective number of observations following *Zwiers and von Storch* [1995].

[12] A wide range in percent iron solubility was observed during this cruise (see Figures 3a and 3b). The average and one standard deviation of Fe_{sol} for the fine and coarse modes was 7 ± 13% and 5 ± 15%, respectively (Table 3). The fine mode solubility was 1.3 times higher than the coarse mode and Fe(II) was predominantly observed in the fine mode (73%) (see Table 4).

[13] During the Pacific cruise (MP02, 9–30 April 2001), total iron concentrations were lower than the MP01 cruise (see Table 2 and Figure 4), and iron was observed equally in both modes (52% in fine mode). Fine and coarse mode iron concentrations were highly correlated with aluminum (r = 0.99).

[14] No major events in solubility were observed during the MP02 Pacific cruise (Figures 5a and 5b). The mean fine and coarse mode values of Fe_{sol} were 1.7 ± 0.8% and 0.6 ± 0.2%, respectively, considerably lower than the MP01 cruise (see Table 3). Fine mode Fe_{sol} was 2.8 times higher than coarse mode Fe_{sol} and Fe(II) concentrations were

Table 2. Observed and Modeled Average Iron Concentrations in the Fine Mode (D_p < 2.5 μm) and Coarse Mode (D_p > 2.5 μm) Listed by Cruise[a]

	Observations, μg m^{-3}		Model (Iron Map), μg m^{-3}		Model (3.5% Dust), μg m^{-3}	
Cruise (2001)	Fine	Coarse	Fine	Coarse	Fine	Coarse
MP01 (Atlantic)	0.3 ± 0.3	0.13 ± 0.15	1.1 ± 1.3	0.14 ± 0.17	1.4 ± 1.7	0.2 ± 0.2
MP02 (Pacific)	0.07 ± 0.09	0.06 ± 0.07	0.06 ± 0.03	0.016 ± 0.008	0.07 ± 0.03	0.018 ± 0.009
MP03 (Atlantic)	0.11 ± 0.11	0.12 ± 0.12	0.7 ± 0.7	0.2 ± 0.3	0.91 ± 1.01	0.3 ± 0.4

[a]The two model estimates correspond to values derived from an iron map and from a dust source map where iron is assumed to be 3.5% dust (see text).

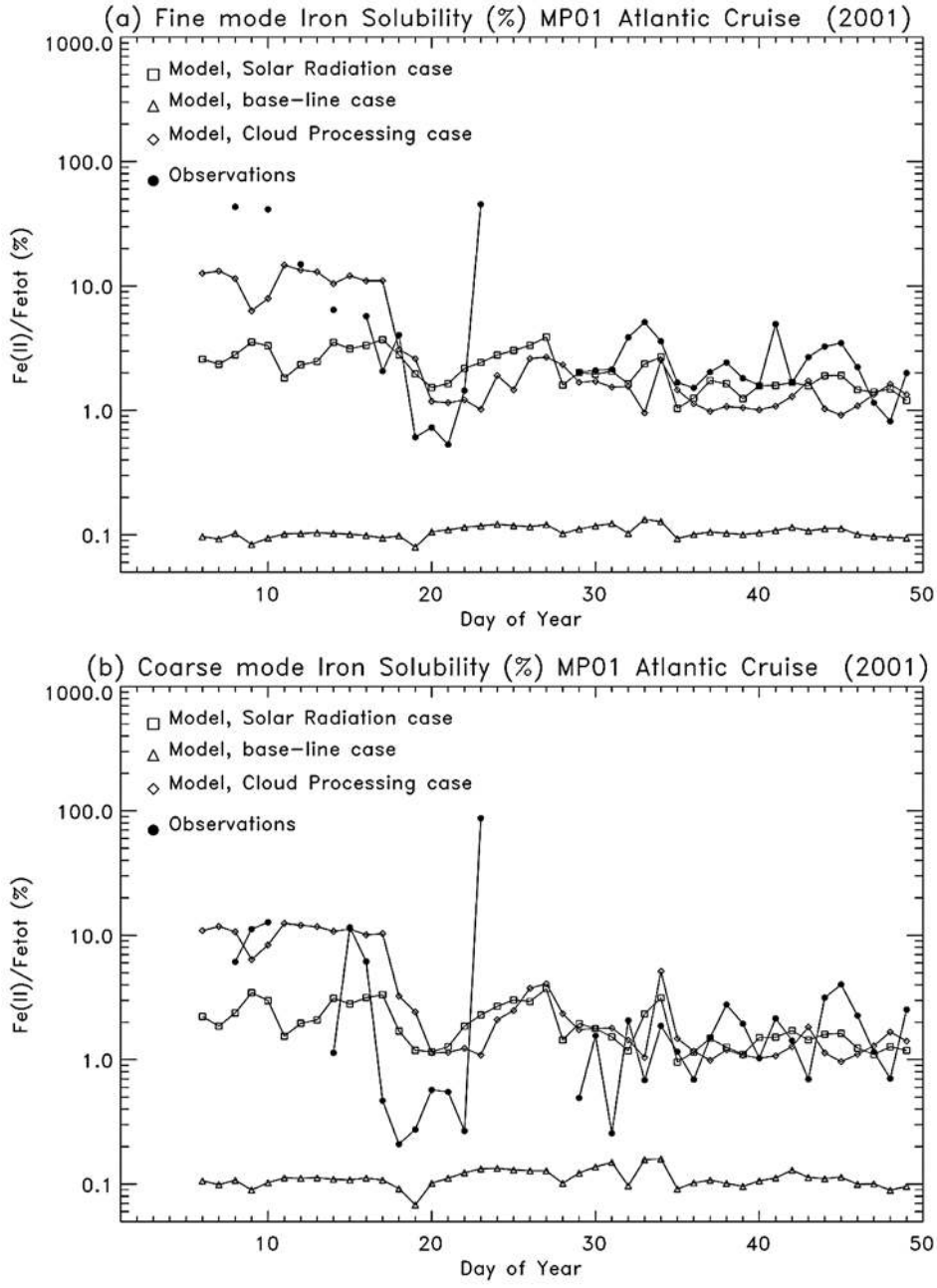

Figure 3. (a) MP01 percent soluble iron (Fe_{sol}, %) from observations and model estimates in the fine mode (diameter <2.5 μm). The model estimates are for a baseline case (no processing), solar radiation (SR) processing, and cloud processing (CP) cases. (b) Same as Figure 3a but for the coarse mode (diameter >2.5 μm).

primarily observed in the fine mode (75%). Mean values of fine and coarse mode Fe(II) concentrations can be found in Table 4.

[15] During the MP03 cruise in the Atlantic (25 June to 19 August 2001), total iron was equally distributed across the fine and coarse modes (48% in fine mode), with mean fine and coarse mode iron concentrations listed in Table 2 (see Figure 6). Fine and coarse mode iron concentrations were highly correlated with aluminum ($r = 0.98$ and $r = 0.97$, respectively). For the majority of this cruise, observed iron solubility was relatively low (Figures 7a and 7b). The fine mode was 14 times more soluble than the coarse mode, with a mean fine and coarse mode Fe_{sol} of 2 ± 7% and 0.2 ± 0.3%, respectively (see Table 3). Fe(II) concentrations were primarily in the fine mode (87%) (Table 4). Although total iron concentrations were equally distributed across the two size modes, enhanced Fe(II) concentrations in the fine mode suggest processes that are more efficient at converting soluble iron at smaller sizes, or differences in composition of the source aerosols. This enhancement is also observed in MP01 and MP02 (see Table 5).

[16] Overall these cruises show a large variability in fine mode iron solubility (4 ± 9%) and fine mode total

Table 3. Observed and Modeled Iron Solubility (Fe_{sol}) for the Fine Mode (D_p < 2.5 μm) and the Coarse Mode (D_p > 2.5 μm)[a]

	Cruise (2001)					
	MP01 (Atlantic)		MP02 (Pacific)		MP03 (Atlantic)	
	Fine	Coarse	Fine	Coarse	Fine	Coarse
Observations, %	7 ± 13	5 ± 15	1.7 ± 0.8	0.6 ± 0.2	2 ± 7	0.2 ± 0.3
Model (BL), %	0.110 ± 0.011	0.11 ± 0.02	0.105 ± 0.005	0.108 ± 0.006	0.096 ± 0.005	0.097 ± 0.006
Model (SR), %	2.2 ± 0.8	2.0 ± 0.8	3.7 ± 0.4	3.0 ± 0.4	3 ± 1	3 ± 1
Model (CP), %	4 ± 5	4 ± 4	10 ± 3	8 ± 2	4 ± 4	4 ± 3
Observations/model (BL)	62.7	45.9	15.9	5.5	24.2	1.8
Observations/model (SR)	3.3	2.8	0.45	0.20	0.67	0.06
Observations/model (CP)	2.1	1.6	0.17	0.07	0.49	0.05
r: observations/model (BL)	0.011	0.16	0.26	−0.006	**0.40**	**0.56**
r: observations/model (SR)	0.44	0.22	−0.16	0.02	0.23	**0.43**
r: observations/model (CP)	0.43	0.03	−0.25	−0.08	**0.35**	**0.70**

[a]Values represent the average and one standard deviation. Model values correspond to the baseline case (BL), the solar radiation case (SR), and the cloud processing case (CP). Ratios of mean observations to mean model values are given, as well as correlation coefficients (*r*). Values that are in bold are significant with a 95% confidence level.

iron amounts (0.2 ± 0.2 μg m^{-3}). The fine mode was 1.6 times more soluble relative to the coarse mode.

2.2. Correlations of Iron Solubility and Aerosol Species

[17] Experimental studies suggest that interactions of iron with other aerosol species in solution could be very important in the enhancement of the bioavailable iron. Specifically, reactions of ferric iron with organic species such as oxalate could play a significant role in producing soluble iron [e.g., *Zuo and Hoigné*, 1992; *Zhu et al.*, 1993; *Pehkonen et al.*, 1993; *Siefert et al.*, 1994; *Zuo*, 1995]. Oxalic acid is common in cloud water, and has anthropogenic sources such as incomplete combustion, ozonolysis and photooxidation of hydrocarbons [*Warneck*, 2003]. *Saydam and Senyuva* [2002] found enhancements of soluble iron through in-cloud photochemical reductions assisted by oxalate and suggested that fungi in the soils were a natural source. Inorganic aerosol solutions can also be important if mineral aerosols are coated with hygroscopic species such as sulfates and nitrates [e.g., *Zhuang et al.*, 1992; *Zhu et al.*, 1992]. Cycles of evaporation and condensation can result in very acidic solutions with high ionic strengths and can enhance the reduction of Fe(III) [*Zhu et al.*, 1997].

[18] Understanding the role of other aerosol species on these reduction reactions involving iron is necessary for recognizing the processes that govern the enhancement of soluble iron and its deposition to the ocean. As *Jickells and Spokes* [2001] suggest, wet deposition is likely to be responsible for the deposition of iron to the oceans, partly due to the large fraction of wet deposited mineral aerosols. Soil mineral surfaces strongly attract water [e.g., *Koretsky et al.*, 1997], and thus are likely to be easily incorporated into cloud water as either CCN or scavenged. Mineral aerosols that are mixed with other hygroscopic species would be more susceptible to removal by precipitation scavenging. Increases in anthropogenic influences that result in higher levels of soluble iron being deposited to the oceans would have important implications for biogeochemical cycles. We investigate the effects of other aerosol species by exploring the relationships between soluble iron and measured aerosol composition, specifically sulfate and oxalate.

2.2.1. MP01: Atlantic Cruise (6 January to 22 February 2001)

[19] Non-sea-salt sulfate (nss-SO_4^{-2}) contributions to total sulfate were determined from measured sodium concentrations and the ratio of sodium and sulfate in seawater (0.252 [*Seinfeld and Pandis*, 1997]). Non-sea-salt sources of sulfate are derived from oxidation of anthropogenic SO_2 and biogenic sources such as oxidation of DMS. On average 83% of nss-SO_4^{-2} was in the fine mode. Of the total SO_4^{-2} in the fine mode, 69% of it is non-sea-salt derived, while for the coarse mode it was much less (28%). It is possible that our estimates of nss-SO_4^{-2} include some biogenic sources. Investigating the methanesulfonic acid (MSA) to nss-SO_4^{-2} ratio to determine the amount of biogenic sulfate was inconclusive [*Johansen et al.*, 1999, 2000].

[20] As suggested by *Zhu et al.* [1993], acidic aerosol solutions can reduce the oxidation of Fe(II) back to Fe(III).

Table 4. Observed and Modeled Fe(II) for Fine Mode (D_p < 2.5 μm) and Coarse Particle Modes (D_p > 2.5 μm)[a]

	Cruise					
	MP01(Atlantic)		MP02(Pacific)		MP03 (Atlantic)	
	Fine	Coarse	Fine	Coarse	Fine	Coarse
Observations	6 ± 6	2 ± 3	1.1 ± 1.2	0.3 ± 0.2	0.6 ± 0.5	0.08 ± 0.10
Model (SR)	18 ± 19	2 ± 2	2 ± 1	0.5 ± 0.2	17 ± 18	5 ± 5
Model (CP)	15 ± 17	2 ± 2	6 ± 2	1.2 ± 0.6	14 ± 15	4 ± 5
Observations/model (SR)	0.28	0.95	0.47	0.64	0.04	0.02
Observations/model (CP)	0.34	0.96	0.19	0.24	0.05	0.02
r: observations/model (SR)	0.72	0.64	0.07	0.10	0.56	**0.58**
r: observations/model (CP)	0.63	0.53	0.19	0.27	0.51	0.33

[a]Values (in ng m^{-3}) represent the average and one standard deviation. Model values correspond to the solar radiation (SR) case and the cloud processing (CP) case. Ratios of mean observations to mean model values are given, as well as correlation coefficients (*r*). Value in bold is significant with a 95% confidence level.

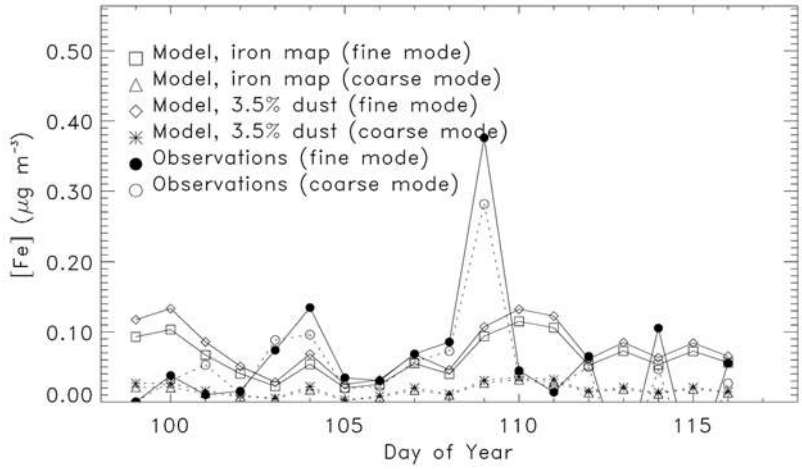

Figure 4. MP02 total iron concentrations ($\mu g\ m^{-3}$) from observations and two model estimates for the fine (diameter <2.5 μm) and coarse particle modes. Model estimates are derived from a dust source map (3.5% of dust is iron) and iron map.

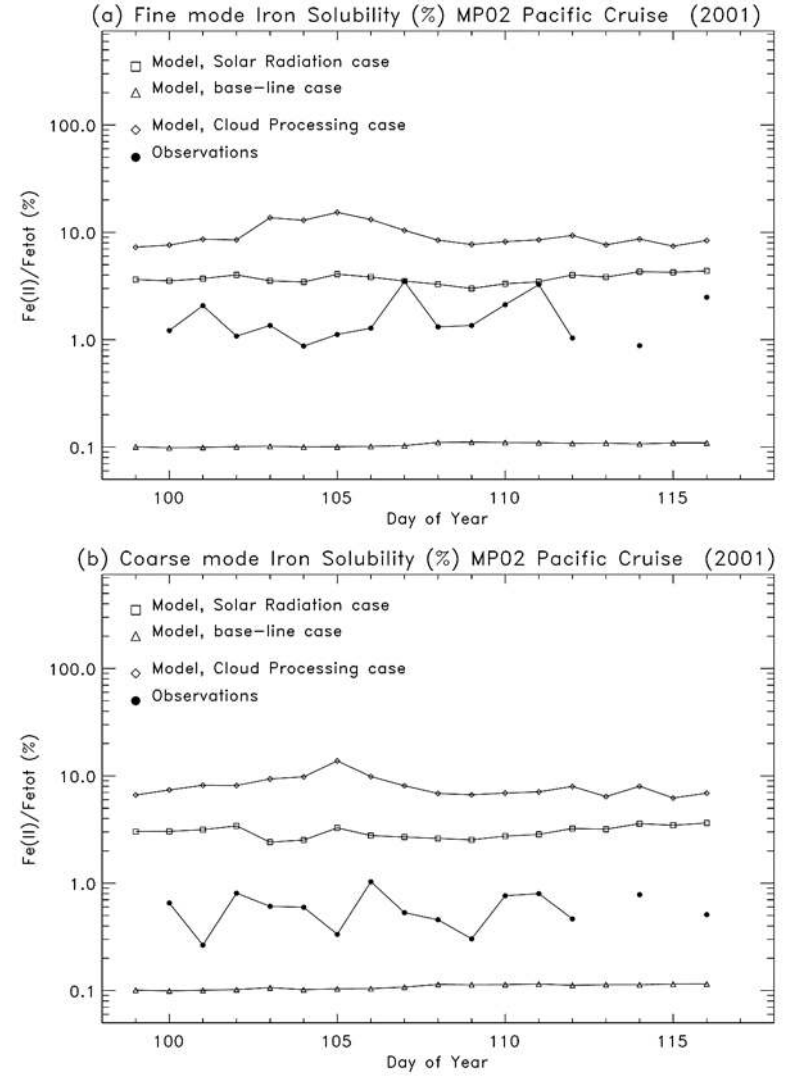

Figure 5. (a) MP02 percent soluble iron (Fe_{sol}, %) from observations and model estimates in the fine mode (diameter <2.5 μm). The model estimates are for a baseline case (no processing), solar radiation (SR) processing, and cloud processing (CP) cases. (b) Same as Figure 5a but for the coarse mode (diameter >2.5 μm).

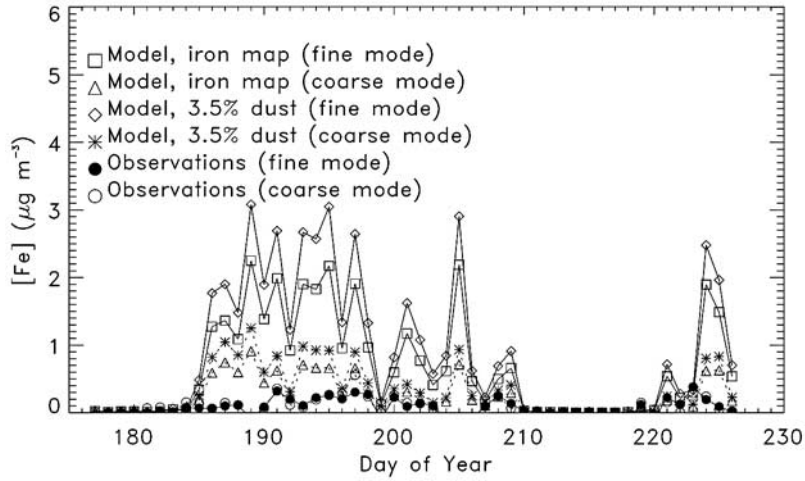

Figure 6. MP03 total iron concentrations ($\mu g\ m^{-3}$) from observations and two model estimates for the fine (diameter <2.5 μm) and coarse particle modes. Model estimates are derived from a dust source map (3.5% of dust is iron) and iron map.

Ammonium often is observed in the fine mode and acts to neutralize acidic species such as sulfate and nitrate. The molar ratio of NH_4^+/nss-SO_4^{-2} is an indication of aerosol acidity and speciation. A value of 0 corresponds to sulfuric acid and a value of 2 indicates the aerosol is fully neutralized $(NH_4)_2SO_4$. The average fine mode ratio during this cruise was 0.6 ± 0.3 (average and one standard deviation), suggesting acidic aerosols. These values do not include the effects of other species that could influence the aerosol acidity, such as non-sea-salt calcium. The coarse mode ratio was not computed because of the uncertainties associated with low nss-SO_4^{-2} concentrations in the denominator. The total (fine and coarse mode) ratio was also 0.6 ± 0.3.

[21] Time series of fine and coarse mode nss-SO_4^{-2} are shown in Figures 8a and 8b, respectively. Weak correlations between fine mode nss-SO_4^{-2} and Fe(II) concentrations and Fe_{sol} suggest the possibility that aerosol interactions played a role in enhancing soluble iron (see Table 6 for correlation coefficients). Coarse mode nss-SO_4^{-2} was not correlated with either Fe_{sol} or Fe(II). No correlations were found between the NH_4^+/nss-SO_4^{-2} ratio and Fe(II) concentrations or Fe_{sol} for either modes; however, on days with high Fe_{sol} (e.g., days 8, 10, 12 and 23), the fine mode molar ratio was low (~0.5). The ship was near the Florida coast for days 8–12 (see Figure 1a), and on day 23 the ship was nearing the coast of South America where anthropogenic influences may be more important.

[22] Oxalate concentrations were not significantly correlated with Fe(II) concentrations or Fe_{sol} in the fine or coarse modes (see Figures 8a and 8b and Table 6). Oxalate and nss-SO_4^{-2} concentrations were significantly correlated in the fine mode, suggesting both may have been anthropogenic in origin (Table 6). It is possible that sulfate, oxalate or other aerosol species may have contributed to the processing of iron during this cruise. The high values of Fe_{sol} observed during the early part of the cruise and on day 23 correspond to higher concentrations of anthropogenic species and more acidic aerosols, conditions that have been shown to enhance soluble iron (although the increased Fe(II) could be due to anthropogenic sources of Fe as well).

2.2.2. MP02: Pacific Cruise (9–30 April 2001)

[23] Aerosol composition during this cruise appeared to be strongly affected by sea salt. Contributions of nss-SO_4^{-2} were very low and composed a small fraction (~20%) of total SO_4^{-2} in each mode. The fine mode NH_4^+/nss-SO_4^{-2} ratio of 0.8 ± 0.3 suggested a less acidic aerosol on average compared to the MP01 cruise. The total (fine and coarse mode) molar ratio was 0.7 ± 0.3. Significant correlations were observed in the fine mode between nss-SO_4^{-2} and Fe(II) concentrations and Fe_{sol}, but not in the coarse mode (see Table 6 and Figures 9a and 9b). Fine mode nss-SO_4^{-2} and Fe_{sol} both increased on day 107 (17 April), and the NH_4^+/nss-SO_4^{-2} molar ratio was relatively low on this day (0.78).

[24] Oxalate and nss-SO_4^{-2} concentrations were correlated in the fine mode, but were not significantly correlated in the coarse mode (see Table 6 and Figures 9a and 9b). A peak in fine mode oxalate occurred on day 107, similarly to nss-SO_4^{-2} and Fe_{sol} (see Figure 9a). On this day the ship was at its furthest point from Hawaii (see Figure 1b). Oxalate concentrations were correlated with Fe(II) concentrations and Fe_{sol} in the fine mode. Although Fe_{sol} was relatively low and stable during this cruise and the aerosol seemed to be predominantly sea salt in origin, the correlations between observed aerosol composition and soluble iron suggest that the available nss-SO4 and oxalic species may have had some role in converting Fe(III) to Fe(II).

2.2.3. MP03: Atlantic Cruise (25 June to 19 August 2001)

[25] Non-sea-salt SO_4^{-2} concentrations were lower on average compared to the MP01 cruise and were predominantly in the fine mode (80%) (see Figures 10a and 10b). Fine mode total SO_4^{-2} was comprised mostly of nss-SO_4^{-2} (70%), suggesting less impact by sea salt than the coarse mode (57%). The NH_4^+/nss-SO_4^{-2} ratio was 0.75 ± 0.5 for both modes combined, corresponding to a relatively acidic aerosol. Neither Fe(II) concentrations nor Fe_{sol} concentrations were correlated with nss-SO_4^{-2} in either mode, nor was there any indication of high nss-SO_4^{-2} on days with high Fe_{sol} (see Table 6 and Figures 10a and 10b).

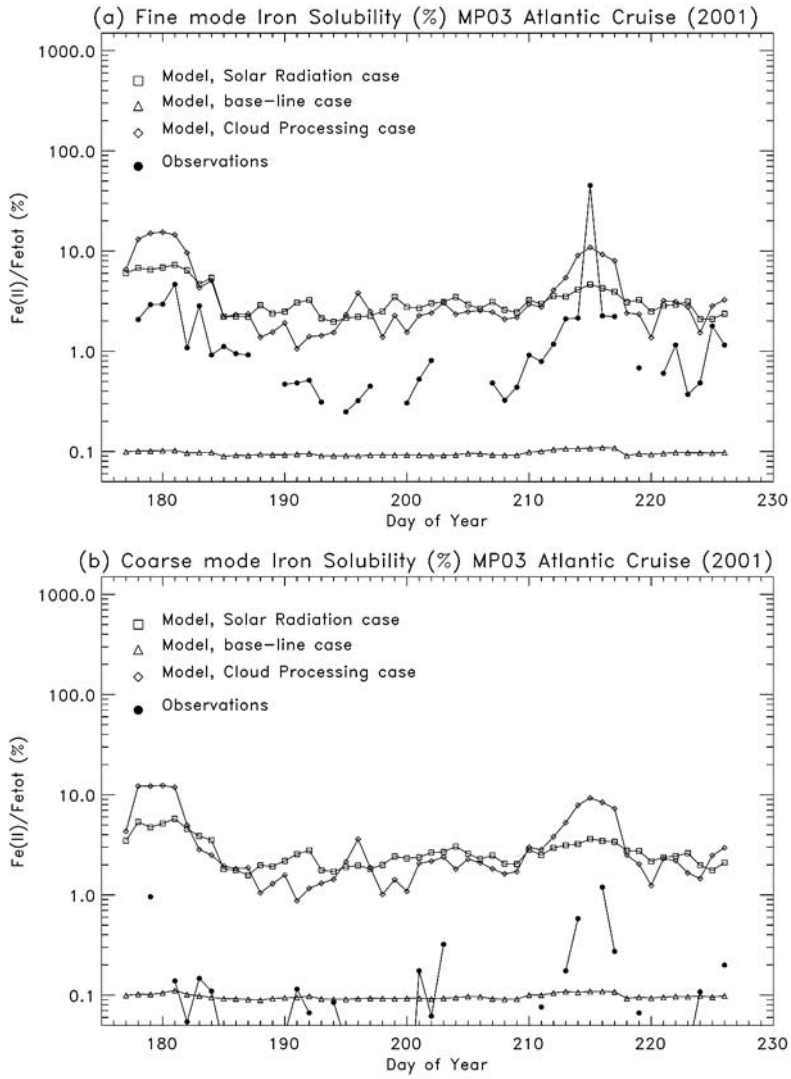

Figure 7. (a) MP03 percent soluble iron (Fe_{sol}, %) from observations and model estimates in the fine mode (diameter <2.5 μm). The model estimates are for a baseline case (no processing), solar radiation (SR) processing and cloud processing (CP) cases. (b) Same as Figure 7a but for the coarse mode (diameter >2.5 μm).

[26] Oxalate concentrations were found predominantly in the fine mode (80%) (see Figures 10a and 10b). Oxalate concentrations were correlated with nss-SO_4^{-2} in the coarse mode but not the fine mode. Fe(II) concentrations and Fe_{sol} were uncorrelated with oxalate in both modes (Table 6).

[27] The combined results from all three cruises demonstrate the complexity of the processes involving iron and other aerosol species. In fact, no consistent picture emerges to reveal the role of aerosol species in iron processing. It is interesting that the cruise with the highest correlations between iron solubility and aerosol species (MP02) in fact never had any high solubility "events" compared to the other cruises. However, as experimental studies have shown, the necessary environment for enhancing soluble iron was present for all cruises, namely, acidic aerosol solutions with hygroscopic species that could participate in cloud cycling, and inorganic and organic species of anthropogenic origin.

Table 5. Percent of Total Iron (Fe) and Fe(II) in the Fine Mode for Observations and Modeled Values and Ratios of Fine Mode Fe_{sol} to Coarse Mode Fe_{sol}[a]

Cruise (2001)	Fe Fine Fraction, %		Fe(II) Fine Fraction, %		Fine Fe_{sol}/ Coarse Fe_{sol}	
MP01 observations	68		73		1.3	
MP02 observations	52		75		2.8	
MP03 observations	48		87		14	
	Iron Map	3.5% Dust	SR	CP	SR	CP
MP01 model	89	89	90	89	1.1	1.0
MPO2 model	80	81	83	83	1.2	1.2
MP03 model	72	72	75	77	1.2	1.2

[a]Model total iron fractions are given for the dust map source and the iron map source. Model estimates of Fe(II) and Fe_{sol} are for the solar radiation case (SR) and the cloud processing case (CP).

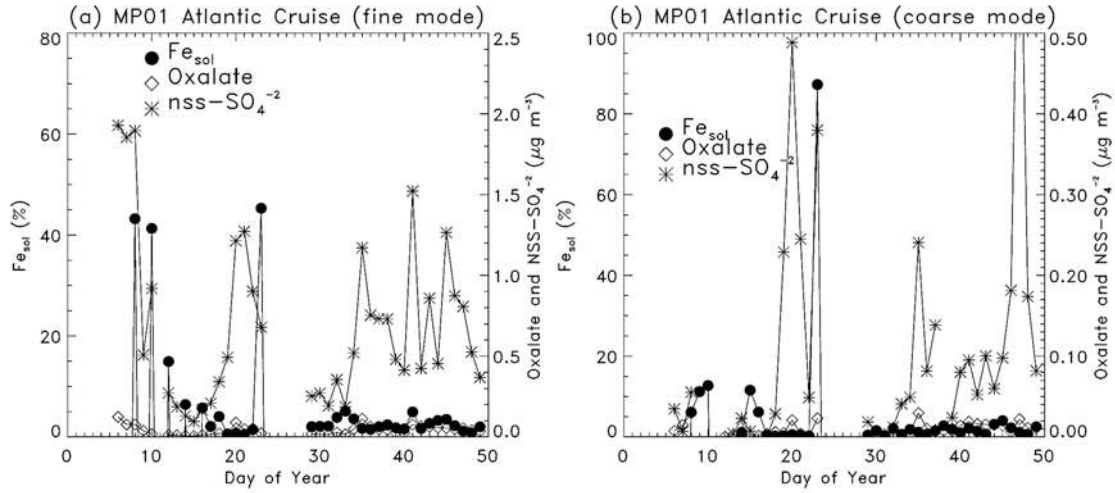

Figure 8. (a) MP01 fine mode nss-SO_4^{-2} and oxalate concentrations on the right axis ($\mu g\ m^{-3}$) and percent soluble iron (Fe_{sol}, %) on the left axis. (b) MP01 coarse mode nss-SO_4^{-2} and oxalate concentrations on the right axis ($\mu g\ m^{-3}$) and percent soluble iron (%) on the left axis.

[28] One relationship evident in observations from all three cruises is the size segregation in iron solubility. On average, fine mode iron solubility was higher than coarse mode iron solubility for all the cruises, and Fe(II) concentrations were predominantly higher in the fine mode (see Table 5). Regardless of the size distribution of total iron in the aerosol, the preferential selection of the fine mode Fe(II) suggests that either the sources of soluble iron were predominantly associated with the fine mode, the fine mode was preferentially selected by the processing, or that the fine mode had a longer atmospheric lifetime and thus was processed longer before being removed. This size segregation is an important result because smaller particles have longer lifetimes, allowing them to be transported to remote regions where total iron deposition is lower, and the ocean biota may be experiencing iron limitation.

[29] In the following sections we present a modeling study designed to investigate the roles of atmospheric processes that enhance iron solubility. With simple assumptions, we investigate size segregation of iron solubility, the importance of photoreduction reactions, and the importance of cloud processes in enhancing soluble iron. Before presenting our modeled iron solubility and comparisons with observations, we first provide a brief description of the model and comparison with surface and remote-sensing observations of total mineral dust.

3. Model Description

[30] The Dust Entrainment And Deposition (DEAD) desert dust module described by *Zender et al.* [2003] and *Mahowald et al.* [2002], coupled with the Model of Atmospheric Transport and Chemistry (MATCH) [*Rasch et al.*, 1997; *Mahowald et al.*, 1997], was used to simulate the global distribution of desert dust in the atmosphere for 2001. MATCH is driven by the National Center for Environmental Prediction/National Center for Atmospheric Research (NCEP) reanalysis meteorology [*Kalnay et al.*, 1996; *Kistler et al.*, 2001] and has a horizontal resolution of T62 ($1.8° \times 1.8°$), a vertical resolution of 28 levels (surface to 10 mbar) and is available every 6 hours.

[31] Entrainment of soil particles in the atmosphere begins with saltation from strong winds over dry and bare soils. Mobilization of the particles into the atmosphere for further transport occurs when a fraction of the horizontal flux is converted to a vertical flux. The mobilization scheme is sensitive to soil wetness, wind velocity and atmospheric stability, and is described further by *Zender et al.* [2003]. The aerosols are characterized by four size bins, ranging in diameter from 0.1 to 1.0 μm, 1.0 to 2.5 μm, 2.5 to 5.0 μm, and 5.0 to 10 μm. Lognormal size distributions are assumed within each size bin. Source mass fractions vary per bin, with 10% for the smallest size bin and 30% for each of the three larger size bins [*Mahowald et al.*, 2002].

[32] Because of insufficient global soil characterization data, we assume soil particles that are optimally sized to initiate saltation, while applying a factor to describe the fraction of the grid box consisting of easily erodible soils. We assume all topographic lows with unvegetated, dry soils are potential source areas and apply the methodology of *Ginoux et al.* [2001] for source areas. No anthropogenic sources were included. The sources described above were used to simulate total dust concentrations in the atmosphere.

Table 6. Correlation Coefficients (r) Between Observed Non-Sea-Salt Sulfate (nss-SO_4^{-2}) and Oxalate Concentrations and Percent Iron Solubility (Fe_{sol}) and Ferrous Iron (Fe(II)) for the Fine ($D_p < 2.5$ μm) and Coarse Particle Modes ($D_p > 2.5$ μm)[a]

	Cruise					
	MP01 (Atlantic)		MP02 (Pacific)		MP03 (Atlantic)	
	Fine	Coarse	Fine	Coarse	Fine	Coarse
nss-SO_4^{-2} and Fe(II)	0.41	0.32	**0.82**	0.07	0.23	0.26
nss-SO_4^{-2} and Fe_{sol}	0.31	0.25	**0.68**	0.23	−0.26	−0.18
Oxalate and Fe(II)	0.58	0.56	**0.82**	**0.78**	−0.05	0.20
Oxalate and Fe_{sol}	−0.09	0.29	**0.69**	−0.43	−0.12	−0.06
Nss-SO_4^{-2} and oxalate	**0.82**	0.50	**0.88**	0.39	0.07	**0.74**

[a]Values in bold are significant with a 95% confidence level.

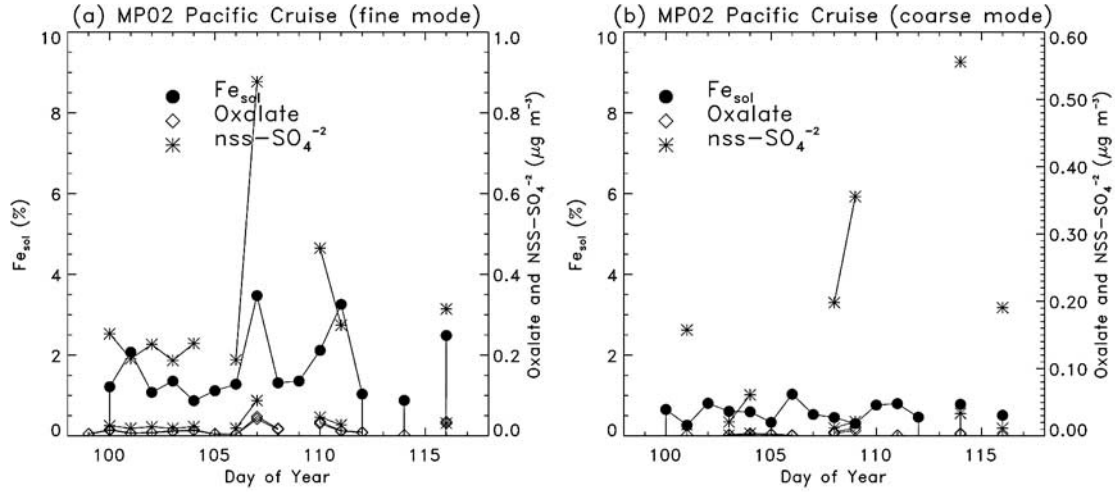

Figure 9. (a) MP02 fine mode nss-SO_4^{-2} and oxalate concentrations on the right axis (μg m^{-3}) and percent soluble iron (Fe_{sol}, %) on the left axis. (b) MP02 coarse mode nss-SO_4^{-2} and oxalate concentrations on the right axis (μg m^{-3}) and percent soluble iron (%) on the left axis.

[33] We used two different source profiles to determine the iron fraction of the mineral aerosols in the model. First, we derived total iron concentrations in the atmosphere by assuming 3.5% of total dust is iron [*Duce and Tindale*, 1991]. The second source profile (referred to as the "iron map") was based on the measurements of soluble iron extracted at a pH of 4.65 from soil samples [*Sillanpää*, 1982], and the global extrapolation of the measurements based on a map of soil types [*Fung et al.*, 2000]. As expected, the extractable soil Fe content decreases with increasing soil pH and $CaCO_3$ equivalents, and increases with texture and organic carbon content. The soil studies show that the iron may exist as coatings on soil particles, as concretions or nodules, and that there is significant transformation of iron in the presence of organic matter and microorganisms. Extractable soil Fe is as low as 0.17% for xerosols and as high as 2.5% for histosols. The map shown in Figure 11 demonstrates sensitivity to sources with varying iron abundance in soils. For example, in the Sahel regions there is approximately twice as much iron in the soils as in the nearby Sahara [*Claquin et al.*, 1999; *Sokolik and Toon*, 1999; *Johansen et al.*, 2000]. The annual average ratio between the iron map and iron derived by assuming iron is a constant 3.5% fraction of total dust is shown in Figure 12. Notice that the twofold difference seen in the source regions has been reduced to a 10% difference over much of the oceans due to the mixing of aerosols from different regions in this model.

[34] Loss processes in the model include both dry and wet deposition, both of which are described in detail by *Zender et al.* [2003]. Dry deposition processes are size dependent and include gravitational settling and turbulent mix out, resulting in lifetimes ranging from 362 days in the smallest size bin to 1.1 days for the largest size bin. Dry deposition

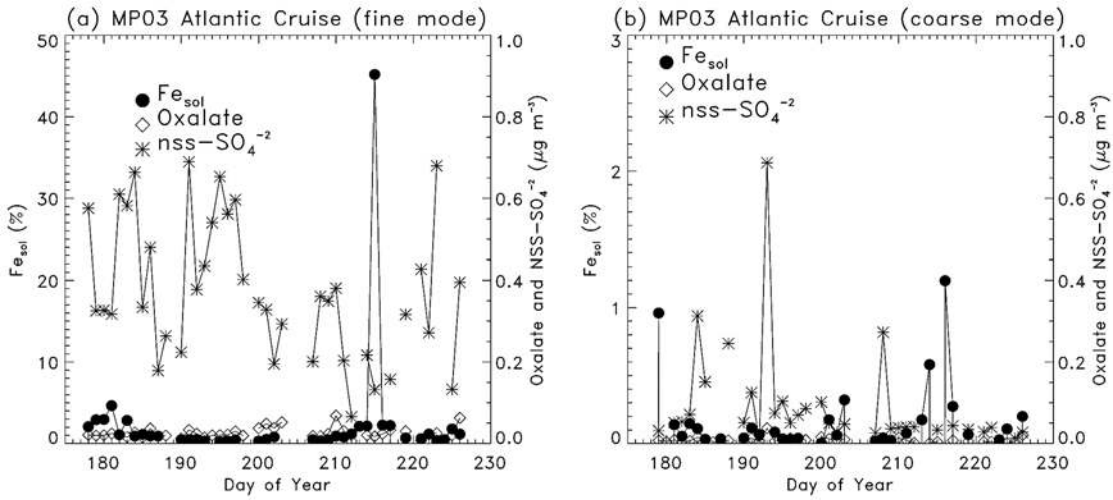

Figure 10. (a) MP03 fine mode nss-SO_4^{-2} and oxalate concentrations on the right axis (μg m^{-3}) and percent soluble iron (Fe_{sol}, %) on the left axis. (b) MP03 coarse mode nss-SO_4^{-2} and oxalate concentrations on the right axis (μg m^{-3}) and percent soluble iron (%) on the left axis.

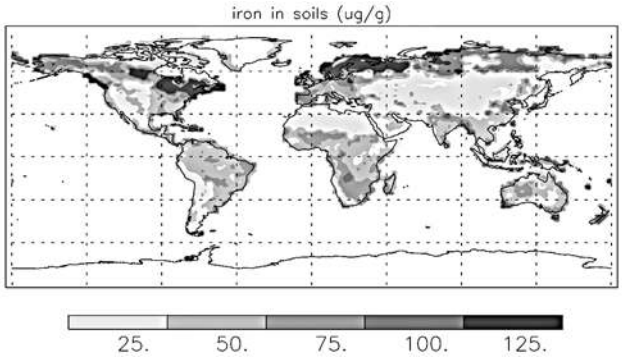

Figure 11. Global map of iron in soils ($\mu g\ g^{-1}$). See text for explanation.

Table 7. Wet Versus Dry Deposition of Mineral Aerosols

Location	Wet Deposition, %		Citation
	Observations	Model	
Bermuda	17–70	75–95	*Jickells et al.* [1998], T. Church (personal communication, 1999), and *Kim and Church* [2001]
Amsterdam Island	35–43	75–95	*Jickells and Spokes* [2001].
Cape Ferrat, Mediterranean	35	50–75	*Guieu et al.* [1997]
Enewetak Atoll	83	75–95	*Arimoto et al.* [1985]
Samoa	83	75–95	*Arimoto et al.* [1987]
New Zealand	53	75–95	*Arimoto et al.* [1990]
North Pacific	75–85	75–95	*Uematsu et al.* [1985]
Summit Greenland	63	50–75	*Davidson et al.* [1996]
Antarctica	90	50–95	*Wolff et al.* [1998]

lifetime for the combined size bins is 10.5 days [*Luo et al.*, 2003]. Wet deposition due to scavenging of particles by water is modeled with a simple scavenging coefficient of 750 kg/kg for convective and stratiform precipitation [*Tegen and Fung*, 1994; *Zender et al.*, 2003]. Wet deposition lifetime is approximately 12 days for each bin. Both the model results and available observations suggest most of the mineral aerosol deposition is due to wet deposition (see Table 7), which is different than the conclusions from *Jickells and Spokes* [2001], perhaps due to the subset of observational data they review. The comparisons of the model results with observations (Table 7) suggest that the model reasonably estimates the fraction of wet deposition versus dry deposition, but may slightly over predict wet deposition. The considerable variability in measured dry versus wet deposition rates (see Table 7) reflects the natural variability in the deposition rates as well as the difficulty in making such measurements.

[35] The MATCH model simulates the hydrological cycle using both moist convective [*Zhang and McFarlan*, 1995; *Hack*, 1994] and stratiform precipitation parameterizations [*Rasch and Kristjánsson*, 1998], similar to those in the NCAR community climate model. These parameterizations have been shown to recreate similar precipitation off line as online [e.g., *Rasch et al.*, 1997] and to simulate similar precipitation patterns as the NCEP reanalyses when driven with NCEP reanalysis winds [*Mahowald et al.*, 1997; *Luo et al.*, 2003]. However, comparisons with observations show that the NCEP reanalysis precipitation does not capture exactly the precipitation in the observations [e.g., *Trenberth and Guillemot*, 1998; *Luo et al.*, 2003]. Thus, while the clouds simulated in MATCH should be similar to those in the reanalysis, there will still be errors in the cloud predictions.

[36] Other studies using MATCH/DEAD/NCEP demonstrate the model is realistically simulating observed desert dust climatologies and capturing annual average concentrations globally over many orders of magnitudes, although it is over predicting surface concentrations at many southern hemisphere locations [*Mahowald et al.*, 2002, 2003; *Luo et al.*, 2003]. Studies have shown the model is sensitive to meteorological data sets incorporated in MATCH [*Luo et al.*, 2003] and to source areas [*Mahowald et al.*, 2002]. Although the model adequately reproduces mean dust concentrations from many observation sites, occasionally it may not capture particular dust "events" in the same time period. In section 3.1 we compare model results to in situ and remote-sensing observations available during 2001 for

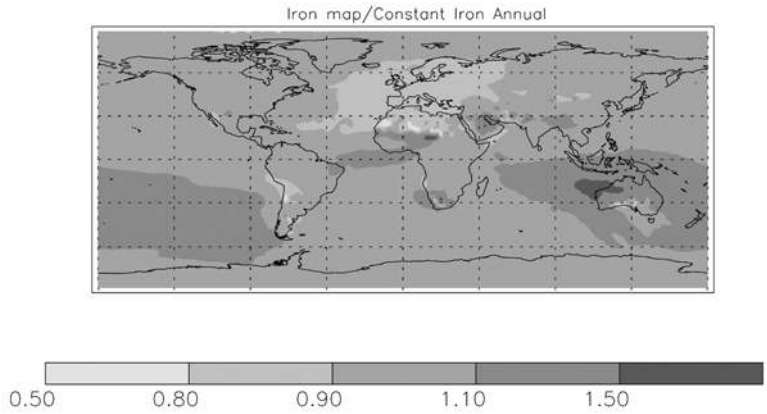

Figure 12. Global map of the ratio of the annual average atmospheric iron concentrations derived from the iron map in Figure 11 to iron concentrations derived from 3.5% dust concentrations.

Table 8. Correlation Coefficients (r) and Ratios of Mean Observed Total Iron Concentrations to Mean Modeled Iron Concentrations for the Fine Mode ($D_p < 2.5$ μm) and Coarse Mode ($D_p > 2.5$ μm)[a]

	Observations/Model				r			
	Iron Map		3.5% Dust		Iron Map		3.5% Dust	
Cruise (2001)	Fine	Coarse	Fine	Coarse	Fine	Coarse	Fine	Coarse
MP01 (Atlantic)	0.22	0.81	0.18	0.66	**0.82**	**0.80**	**0.82**	**0.79**
MP02 (Pacific)	1.3	4.0	1.1	3.5	0.19	0.32	0.15	0.31
MP03 (Atlantic)	0.17	0.5	0.13	0.37	0.60	0.53	0.59	0.53

[a]Modeled iron concentrations were derived using a dust map (iron is 3.5% of dust) and an iron map. Values that are in bold are significant with a 95% confidence level.

the time periods and locations of the MANTRA and PIRANA cruises.

3.1. Comparisons Between the Model and Cruise-Based Observations

[37] The model over predicted total iron concentrations compared to observations for the Atlantic Ocean cruises (MP01 and MP03) (see Table 8 and Figures 2 and 6). In general, simulations with the iron map resulted in lower concentrations of total iron compared to the estimates derived assuming 3.5% of total dust is iron. The correlation coefficients for comparisons between the model estimates and observations during the Pacific cruise (MP02) were not significant and on average the model under predicted total iron for this case (see Table 8 and Figure 4). The model appears to over predict the fraction of iron in the fine mode for all cruises (Table 5).

[38] Aluminum was derived from the model results by assuming 7% of the total dust is aluminum [*Prospero*, 1999]. The comparisons of aluminum concentrations between the model and observations mirror the iron concentration comparisons (not shown), with the model over predicting aluminum concentrations on average (see Table 9). Ratios of iron to aluminum assumed in the model (Fe/Al = 0.5) were similar to observed values on average, especially for the Atlantic Ocean cruises (see Table 9). These average observed ratios suggest impact from northern Saharan regions that have Fe/Al ratios ranging from 0.3 to 1.1 [*Johansen et al.*, 2000]. *Falkovich et al.* [2001] obtained values of 0.7 ± 0.3 from single particle analysis of North African dust. Observed values of Fe/Al in the Pacific Ocean region were slightly higher than the model (see Table 9).

3.2. Comparisons Between the Model and Remote-Sensing Observations

[39] We incorporate measurements from the Moderate Resolution Imaging Spectroradiometer (MODIS) on board the Earth Observing System (EOS) Terra satellite that acquires daily global observations in 36 spectral bands (0.4–1.4 μm) at three spatial resolutions (250, 500, and 1 km) [*Chu et al.*, 2002]. Aerosol optical depth (τ_{aer}) is retrieved over vegetated land at wavelengths of 0.47 and 0.66 μm and over ocean at wavelengths of 0.47, 0.55, 0.66, 0.87, 1.2, 1.6, and 2.1 μm. Several studies have validated MODIS retrievals with ground based remote sensing networks such as AERONET [*Remer et al.*, 2002; *Chu et al.*, 2002; *Ichoku et al.*, 2002a; *Martins et al.*, 2002; *Levy et al.*, 2003] and have demonstrated that MODIS is performing within experimental uncertainties ($\Delta\tau_{aer} = \pm 0.03 \pm 0.05\tau_{aer}$ over ocean and $\Delta\tau_{aer} = \pm 0.05 \pm 0.2\tau_{aer}$ over land from *Remer et al.* [2002] and *Chu et al.* [2002], respectively). We used MODIS retrievals over ocean to validate model-derived dust aerosol optical depths at cruise track locations. We also include τ_{aer} measured by Microtops II Sun photometer on board the cruises.

[40] To account for differences in spatial and temporal resolutions between the model and satellite observations, the MAPSS method (MODIS Aerosol and associated Parameters Spatio-temporal Statisitics) for computing spatial and temporal statistics described by *Ichoku et al.* [2002a] was used to compare MODIS level 2 (ungridded) τ_{aer} with cruise-based Sun photometer data and model results. The satellite overpass must exist within a 50 × 50 km window of the ground-based measurement, corresponding to approximately an hour of the surface-based measurement segment [*Ichoku et al.*, 2002a]. A small number of MODIS level 2 observations agreed spatially and temporally with the cruise locations due to orbital parameters or cloud or glint contamination, so comparisons are for MP01 and MP03 cruises only.

[41] Retrieved τ_{aer} represents total aerosol, whereas model-derived values correspond only to mineral aerosols. Other aerosol types may be present but not represented in the model; however, in the remote ocean regions of interest in this study, they are assumed to be insignificant (with perhaps the exception of sea salt). Nonsphericity of dust particles can cause artifacts in aerosol retrievals [*Mishchenko et al.*, 1995; *Dubovik et al.*, 2002] and has not been fully quantified or corrected for MODIS or Sun photometer retrievals. Specifically, discrepancies in the spectral variation of τ_{aer} have been shown to exist in dusty conditions, and in these conditions, MODIS τ_{aer} values agreed more closely with Sun photometer measurements at a wavelength of 660 nm [*Levy et al.*, 2003], so our comparisons were performed at this wavelength.

[42] Model τ_{aer} values were derived by multiplying the column-integrated dust concentrations by extinction coefficients at the appropriate wavelengths for each bin and then combining all bins for total aerosol optical depth (see *Zender et al.* [2003] for dust optical properties). The model and Sun photometer comparisons were made at a wavelength of 0.675 μm, and the model and MODIS comparisons were made for a wavelength of 0.66 μm. During the MP01 and MP03 cruises, τ_{aer} from the Sun photometer, model, and MODIS were all significantly

Table 9. Correlation Coefficients (r) and Ratios of Mean Observed Aluminum Concentrations to Mean Modeled Aluminum in the Fine Mode ($D_p < 2.5$ μm) and Coarse Mode ($D_p > 2.5$ μm)[a]

	Observations/ Model (7% Dust)		r		Fe/Al	
Cruise (2001)	Fine	Coarse	Fine	Coarse	Fine	Coarse
MP01 (Atlantic)	0.16	0.63	**0.81**	**0.78**	0.55	0.53
MP02 (Pacific)	0.87	2.8	0.15	0.29	0.61	0.61
MP03 (Atlantic)	0.12	0.38	0.55	0.47	0.54	0.48

[a]Mean iron to mean aluminum ratios are also given. Values that are in bold are significant with a 95% confidence level.

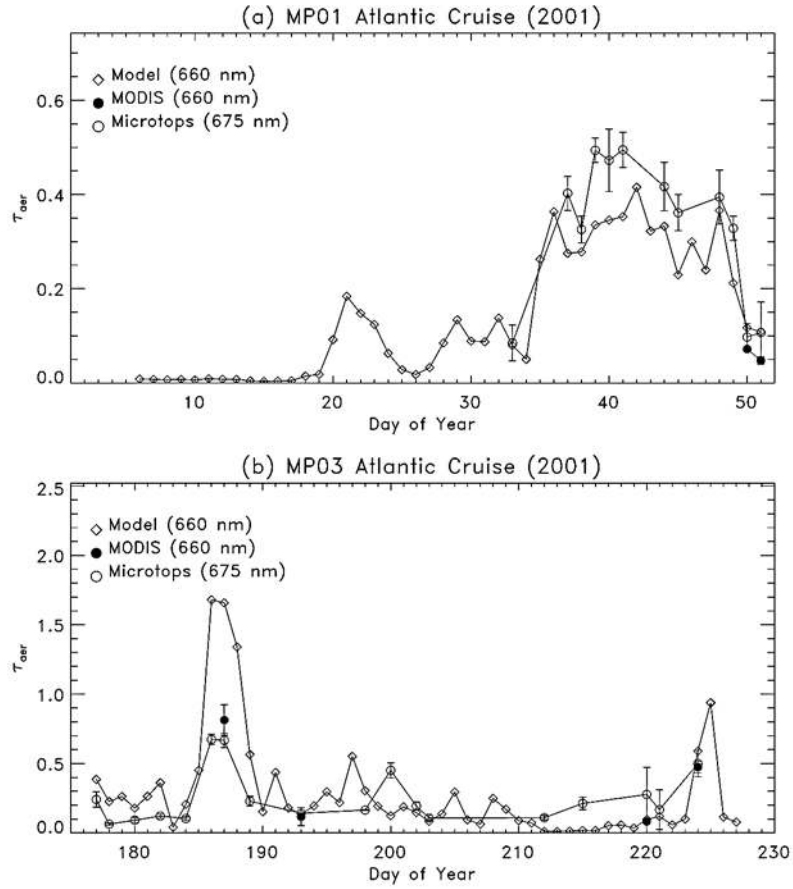

Figure 13. (a) MP01 aerosol optical depth (τ_{aer}) for model (660 nm) and Microtops Sun photometer (675 nm). Two days of MODIS L2 (660 nm) measurements are included. (b) MP03 aerosol optical depth (τ_{aer}) for model (660 nm), Microtops Sun photometer (675 nm), and MODIS L2 (660 nm).

correlated (see Figures 13a and 13b and Table 10). During the MP01 cruise, aerosol optical depths increased around day 35 (4 February) and decreased near day 50 (19 February), similar to total iron concentrations. MODIS τ_{aer} are also low during the end of this cruise. During the MP03 cruise, observed and modeled τ_{aer} peaked on days 186 and 187 (5 and 6 July) and then remained low for the remainder of the cruise, a somewhat different pattern than total iron concentrations. Error bars corresponding to the Microtops data represent one standard deviation for several (at least 10) successive measurements. *Ichoku et al.* [2002b] describe some of the errors and uncertainties inherent in measurements with Microtops II Sun photometers. The error bars associated with MODIS retrievals represent the spatial statistics obtained from the MAPSS method.

3.3. Comparisons Between the Model and Surface-Based Observations

[43] We used data from four surface stations in the region of the cruise tracks for further validation of the model dust concentrations in addition to the comparisons conducted in previous studies [*Luo et al.*, 2003; *Mahowald et al.*, 2003]. The long-term data set from Barbados (13.25°N, 59.5°W, data courtesy D. Savoie) has been incorporated in numerous dust modeling and observational studies [e.g., *Prospero and Nees*, 1986; *Husar et al.*, 1997; *Zhu et al.*, 1997; *Li-Jones and Prospero*, 1998; *Prospero*, 1999; *Guelle et al.*, 2000;

Table 10. Correlation Coefficients (r) and Ratios of Mean Aerosol Optical Depth From Remote Sensing and Model Estimates[a]

Cruise (2001)	Correlation Model-Microtops (λ = 675 nm)	Correlation Model-MODIS (λ = 660 nm)	Correlation MODIS-Microtops (λ = 660, 675 nm)	Microtops/Model	Model/MODIS	Microtops/MODIS
MP01 (Atlantic)	**0.95** (N = 12)	NA	NA	1.3	NA	NA
MP02 (Pacific)	NA	NA	NA	NA	NA	NA
MP03 (Atlantic)	**0.83** (N = 18)	**NA**	**NA**	0.66	0.59	0.94

[a]The wavelength at which the comparison was made is given. The number of observations included in the comparison is N. NA is not applicable. Values that are in bold are significant with a 95% confidence level.

Table 11. Correlation Coefficients (r) and Ratios of Mean Observed Surface Dust and Iron Concentrations to Mean Model Estimates for 2001[a]

Location	Dust OBS/Model	Iron OBS/Model		Dust Correlation	Iron Correlation	
		Soil Map	3.5% Dust		Iron Map	3.5% Dust
Barbados (N = 287)	0.47	NA	NA	**0.43**	NA	NA
Virgin Islands (N = 108)	0.2	0.47	0.37	**0.62**	**0.63**	**0.63**
Haleakala, Hawaii (N = 109)	0.35	0.87	0.82	**0.39**	**0.24**	**0.24**
Hawaii Volcanoes, Hawaii (N = 108)	0.18	0.28	0.26	0.23	**0.3**	**0.29**

[a]With the exception of Barbados, comparisons are for $PM_{2.5}$ concentrations. Modeled iron concentrations were derived using a dust map (iron is 3.5% of dust) and an iron map. The number of observations is given by N, and values in bold are significant at 95%.

Ginoux et al., 2001; *Mahowald et al.*, 2002, 2003]. Comparisons of daily averaged observed total dust concentrations to model results in 2001 suggest the model performs reasonably well in predicting daily dust concentrations, but results in higher concentrations on average (see Table 11). The model is able to capture specific events (e.g., days 100–110, 10–20 April in Figure 14). Increased dust concentrations observed during the MP01 cruise on days 35–50 (4–19 February) are also observed at Barbados, as well as elevated concentrations during the MP03 cruise on days 185–210 (4–29 July) and days 220–230 (8–18 August), suggesting overall dusty conditions in the Atlantic region during these periods. Observed climatological means suggest that during 2001 dust concentrations in Barbados were lower than average in summer and higher than average in autumn. The model dust concentrations tend to agree with the observation climatology in Barbados from 1979 to 2000 [*Luo et al.*, 2003], but the discrepancies in 2001 suggest that the year 2001 is not as well simulated as other years.

[44] The IMPROVE network (Interagency Monitoring of Protected Visual Environments [*Malm et al.*, 1994]) has been measuring aerosol composition at several class 1 areas in the United States since 1988. The network currently operates over 160 sites with $PM_{2.5}$ (particles with aerodynamic diameters less than 2.5 μm) aerosol speciation and PM_{10} total mass concentrations available from 24-hour twice-weekly samples. Estimates of mineral soil concentrations are computed from a soil formula that combines the masses of crustal elements (e.g., Al, Ca, Fe, Si, and Ti) in their normal oxides using molar correction factors. Descriptions and justifications of this soil formula are provided by *Malm et al.* [1994]. IMPROVE $PM_{2.5}$ concentrations have been the focus of several studies investigating the long-range transport of dust to the United States [*Perry et al.*, 1997; *Guelle et al.*, 2000; *Husar et al.*, 2001; *Hand et al.*, 2002; *VanCuren and Cahill*, 2002; *VanCuren*, 2003].

[45] The Virgin Island site (18.34°N, 64.80°W) has been operating since 1990. We use iron as a more direct comparison with the model to remove any discrepancies due to assumptions in soil composition. Model iron concentrations were derived assuming 3.5% of the dust is iron and from the iron map discussed in section 3. The first two model bins were summed to represent $PM_{2.5}$ concentrations. Both model estimates of iron had similar correlations with the observations during 2001 (see Figure 15 and Table 11), but the model estimates from the iron map were closer in magnitude on average than the dust-derived iron estimate. Elevated dust concentrations were observed at the Virgin Island site during the same time periods described in the Barbados comparison, and lower than average concentrations were observed during 2001 compared to its climatological average. Whether the model is reasonably predicting specific events is difficult to determine as the IMPROVE data exist only twice weekly. General agreement of model dust concentrations with observations at the Virgin Island site, the Barbados site, and the cruise observations suggests

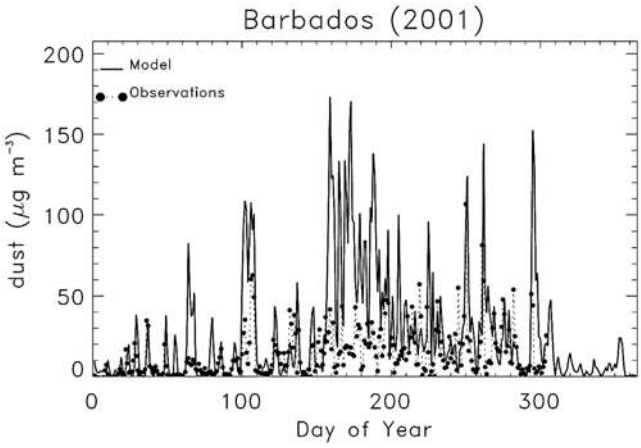

Figure 14. Daily Barbados observations (2001) of total dust and model estimates (μg m^{-3}).

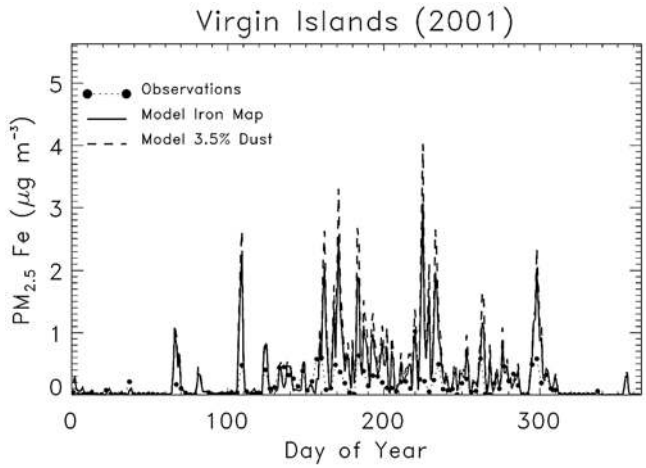

Figure 15. Twice-weekly Virgin Island observations (2001) from the IMPROVE network and daily model estimates of $PM_{2.5}$ iron concentrations (μg m^{-3}). Model estimates include iron derived from a dust source map and from an iron map.

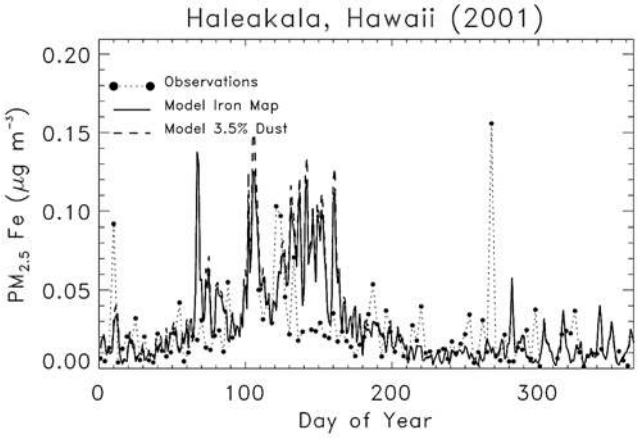

Figure 16. Twice-weekly observations (2001) at Haleakala National Park, Hawaii, from the IMPROVE network and daily model estimates of $PM_{2.5}$ iron concentrations ($\mu g\ m^{-3}$). Model estimates include iron derived from a dust source map and from an iron map.

that the model is performing realistically in the Atlantic Ocean region.

[46] In the Pacific we compare model results to two IMPROVE sites in Hawaii. Haleakala National Park (20.81°N, 156.28°W), on the island of Maui, has been operating since 1991 and historically has a typical Asian dust springtime pattern [*VanCuren and Cahill*, 2002], and comparisons of soil concentrations to a climatological average suggest higher than average soil concentrations at the Hawaii sites during the spring of 2001 (Figure 16). The IMPROVE $PM_{2.5}$ iron and both cases of model iron results were weakly correlated and were within 20% in magnitude on average (Table 11). Weak correlations were also computed for Hawaii Volcanoes National Park (19.43°N, 155.26°W), on the island of Hawaii; however, the model results were higher than the observations at this site as shown in Figure 17. Reasons for the poorer comparisons between model and observations in the Pacific compared to the Atlantic region may be due to offsets in the timing of events at the Pacific sites, for example the iron concentrations peak on day 120 (30 April) at the Hawaii Volcanoes site and the model peaks around day 105 (15 April). Comparing model dust concentrations with IMPROVE soil concentrations instead of iron concentrations increased the correlation at the Haleakala site and decreased the correlation at the Hawaii Volcanoes site (Table 11). The IMPROVE concentrations for iron and soil were lower at the Hawaii Volcanoes site compared to the Haleakala site (see Figures 16 and 17), although they were weakly correlated ($r = 0.78$ and $r = 0.57$ for soil and iron, respectively).

[47] Overall the model simulation shows some skill in simulating the gradients and events observed in the data, but the model over predicts concentrations in both the Atlantic and Pacific basins during 2001, although climatological comparisons suggest better results [*Luo et al.*, 2003] for reasons not understood. Comparisons between the model and climatological observations for the Pacific suggest much higher skill during the average 1979–2000 than seen in 2001 [*Luo et al.*, 2003]. These comparisons also suggest that the modeled amount of fine mode particles is too high, which is also consistent with recent observations by *Grini and Zender* [2004]. Comparisons to other models [*Ginoux et al.*, 2001] suggest the fraction of small particles used in the source distribution is also probably too high. Future versions of the model will use size distributions that are more consistent with these observations.

4. Modeled Iron Solubility

[48] We shift now from validating the model performance during 2001 to applying it in iron solubility experiments. The results are derived from very simplistic methods assumed to play a role in the processing of soluble iron in the atmosphere. The first method explores the possibility that as insoluble iron is exposed to sunlight it becomes more soluble through photoreduction reactions, as demonstrated in experimental work [e.g., *Pehkonen et al.*, 1993]. The second method examines the enhancement of soluble iron through the effects of cloud processing. In these studies we test whether photoreduction or cloud processing hypotheses can explain both the observed size segregation in percent solubility as well as the variability in and magnitude of percent solubility. As previous studies suggest, the effects of other aerosol species on the enhancement of soluble iron could be significant [*Zuo*, 1995; *Zhu et al.*, 1997]. We did not include these effects; at this time we are limited to only simulating mineral aerosols and not their interaction with other species. In addition, no consistent correlations were observed between aerosol species and percent solubility from the in situ data for all cruises (section 2.2). However, in all cases acidic aerosols were present, but observations did not provide definitive evidence of enhanced iron solubility as a result.

[49] The baseline percent soluble iron is derived from the iron map and total iron derived from dust simulations (3.5% of total dust). These simulations provide estimates of solubility for the case with no atmospheric processing, and were typically around 0.1%, consistent with iron solubility in soils. The variability in the baseline estimates

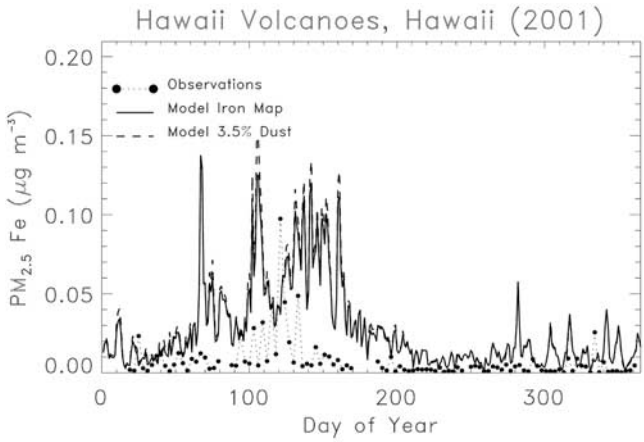

Figure 17. Twice-weekly observations (2001) at Hawaii Volcanoes National Park, Hawaii, from the IMPROVE network and daily model estimates of $PM_{2.5}$ iron concentrations ($\mu g\ m^{-3}$). Model estimates include iron derived from a dust source map and from an iron map.

reflects the differences in sources from the iron map and the dust sources (see Figures 11 and 12).

[50] To estimate the effects of exposure to solar radiation on iron solubility, we assume that exposing insoluble iron to available solar radiation will result in some conversion to soluble iron during daylight hours as suggested by *Siefert et al.* [1997] and *Zhu et al* [1997]. We applied an *e*-folding timescale of 300 days that fell within the range of values observed in the measurements ($\sim$2–20% solubility, see section 2), assuming maximum solar radiation and clear skies, so the modeled timescale will be longer. We assumed a transport time of 7–28 days for mineral aerosols to travel across the Atlantic Ocean from desert dust sources in Africa to the cruise locations [*Husar et al.*, 1997]. The decay rate was computed by

$$\kappa_{SR} = \sum_{i,j} \frac{F_{i,j}}{F_{avg}} \frac{1}{\tau_{SR,sol}} \quad (1)$$

where κ_{SR} (s^{-1}) corresponds to every latitude and longitude grid point (i, j) in the model and is constant with height, $\tau_{SR,sol}$ is the soluble decay lifetime (300 days), $F_{i,j}$ is the shortwave flux at the surface at every location, and F_{avg} is the global mean shortwave flux (535.25 W m^{-2}). The decay acts on all size bins equally. Soluble iron was computed by multiplying the insoluble iron by the decay factor for each time step at each grid point in the model. Therefore locations with high concentrations of dust and high values of shortwave flux would see the largest conversions to soluble iron. After reaching equilibrium in the model, the global mean decay lifetime for each size bin in the model was approximately 700 days.

[51] We estimated the effects of cloud processing on soluble iron by assuming that conversion to soluble iron occurred when insoluble iron came into contact with a cloud [*Siefert et al.*, 1997; *Saydam and Senyuva*, 2002]. The decay factor (κ_{cld}) was computed with

$$\kappa_{cld} = \sum_{i,j} \frac{C_{i,j}}{C_{avg}} \frac{1}{\tau_{cld,sol}} \quad (2)$$

where $C_{i,j}$ represents the fraction of a grid box in cloud at every grid latitude and longitude in the model and at each level, and C_{avg} is the average fraction in the tropics around 10°N (C_{avg} = 0.05). All size bins were treated equally. The soluble decay lifetime ($\tau_{cld,sol}$) was 300 days (assuming clouds always exist with dust, so that the modeled lifetime will be longer). At equilibrium the global mean decay lifetime from these processes was between 370 and 580 days, with longer estimates corresponding to larger size bins. The estimates of soluble iron derived with these methods are clearly sensitive to the values of decay lifetime and parameters involved in the calculation of decay rates; however, given that these values are derived from observations, they represent realistic and simple assumptions.

[52] Model estimates from the baseline case and the two iron solubility processes are shown with observations in Figures 3a, 3b, 5a, 5b, 7a, and 7b, and the mean values of Fe_{sol} for each size mode are given in Table 3. The baseline model estimates under predict iron solubility for all cruises and are significantly correlated only for the MP03 cruise, while the solar radiation (SR) and cloud processing (CP) cases under predict iron solubility for the MP01 cruise, and over predict Fe_{sol} for the MP02 and MP03 cruise. If outliers in Fe_{sol} are removed from the average observed values during the MP01 cruise, the model estimates (both SR and CP) agree in magnitude with the measured values and are weakly correlated for both methods (see Table 3). On average the CP method resulted in higher values (up to triple the amount) of percent iron solubility compared to the SR case, especially during certain time periods (e.g., through day 20 for the MP01 cruise, see Figure 3a), most likely due to increased cloud cover, as TOMS reflectivity and MODIS images suggest. None of the model simulations captures the overall variability in solubility observed in the data, suggesting either that the model is unable to capture cloudiness and insolation variability, or that other processes are important.

[53] These comparisons raise several questions regarding the processes that enhance soluble iron. Similar distributions of Fe(II) concentrations in the fine and coarse modes in the observations and the model results (not shown) suggest that transport and removal has a significant effect on this distribution and may explain the observed higher solubility in the fine mode fraction. However, the observations do show periods when coarse Fe_{sol} is significant (e.g., MP01, Figure 3b), so perhaps other processes, or fast transport of dust to the measurement locations, are important.

[54] The model Fe_{sol} values resulting from exposure to solar radiation and from cloud processing are similar in magnitude to observations at several locations and periods; however, these mechanisms alone do not capture measured events or even the observed variability. While comparisons of the observed aerosol species and Fe_{sol} do not demonstrate consistent correlations, an important aspect of both the photochemical pathway for reduction and cloud processing mechanisms is the presence of other aerosol species, and they were not included in these simulations.

5. Global Implications

[55] Comparisons of simulated percent soluble iron to observations shown in section 4 suggest that other processes need to be understood before we can correctly simulate the observed soluble iron. However, even the variability simulated in section 4 can be useful to consider globally, as a contrast to the simple approaches to soluble iron taken in previous studies. For example, *Fung et al.* [2000] assumed two different percent iron solubilities (1% and 10%) in their simulations, *Duce and Tindale* [1991] used a constant value of 10%, and *Gao et al.* [2003] applied a range 10–50% for wet deposition and 1–6% for dry deposition. Simulated percent soluble iron estimates suggest both cloud processing and photoreduction reactions are important globally. Annually averaged surface global maps of percent iron solubility for the solar radiation case (SR) are shown in Figures 18a and 18b for fine and coarse modes, respectively, as simulated for the year 2001. The lowest values of percent Fe_{sol} occur close to source regions, consistent with low solubility of crustal sources. There are stronger north-south gradients in the Atlantic Ocean compared to the Pacific Ocean,

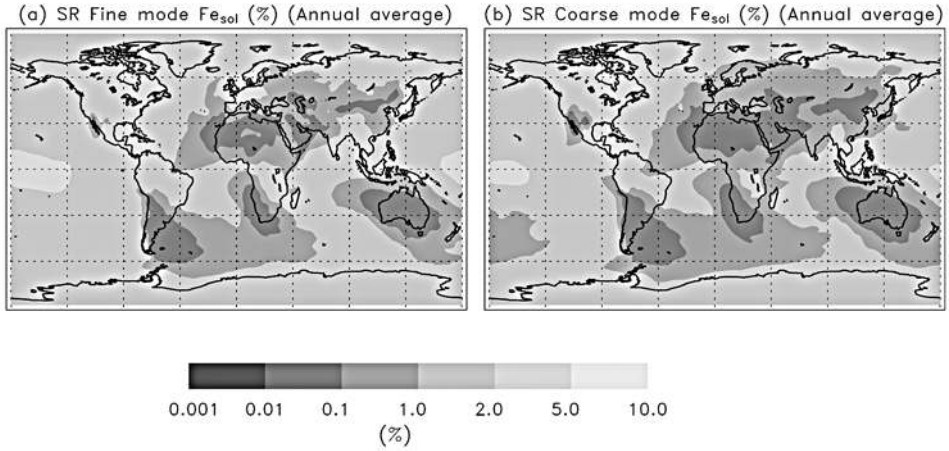

Figure 18. (a) Fine mode annually averaged (2001) global percent iron solubility (Fe_{sol}, %) estimates derived from the solar radiation processing case. (b) Same as Figure 18a but for the coarse particle mode.

although there is a tropical region of higher percent solubility in the Pacific Ocean. The fine mode percent solubility is higher than the coarse mode globally, except near source regions where it is roughly the same, most likely due to the shorter lifetimes of larger particles.

[56] Similar maps of global percent iron solubility for the cloud processing case (CP) are shown in Figures 19a and 19b for fine mode and coarse mode particles, respectively. Values of Fe_{sol} for the CP case range near 10% for much of the globe. Smaller values are observed near source regions and a strong north-south gradient exists in the Atlantic Ocean with higher values toward the poles. Coarse mode Fe_{sol} values are smaller than the fine mode values but with a similar geographical distribution as the fine mode.

[57] The fine mode geographical distribution of Fe_{sol} is similar for the SR and CP cases (higher Fe_{sol} nearer source regions) although the CP case has higher values. Coarse mode Fe_{sol} values are higher for the CP case, except over desert regions where solar radiation is plentiful and cloud cover is minimal. Figures 18 and 19 suggest that percent iron solubility is higher on an annual mean in HNLC regions (subarctic and equatorial Pacific and Southern Oceans) compared to other regions. Although deposition of dust to these regions is low [e.g., *Fung et al.*, 2000], it is possible that conditions with low total iron concentrations correspond to mineral aerosols with long lifetimes that could participate in considerable iron processing. Qualitatively comparing the observed values of Fe_{sol} from Table 1 suggests that the fine mode model geographical distributions are realistically representing measured values around the globe; however, this agreement may be due to the wide range of values measured and different sampling years.

6. Summary

[58] Iron solubility was measured aboard three cruise ships in the equatorial Atlantic and Pacific Oceans in 2001. Percent solubility ranged from 0 to 45% in the fine mode and 0 to 87% in the coarse mode. On average, fine mode percent solubility was higher than coarse mode solubility for all cruises. Comparisons of observed percent solubility with measured sulfate and oxalate concentrations did not demonstrate consistent correlations. As mentioned in section 1, we use only Fe(II) in the definition of Fe_{sol}.

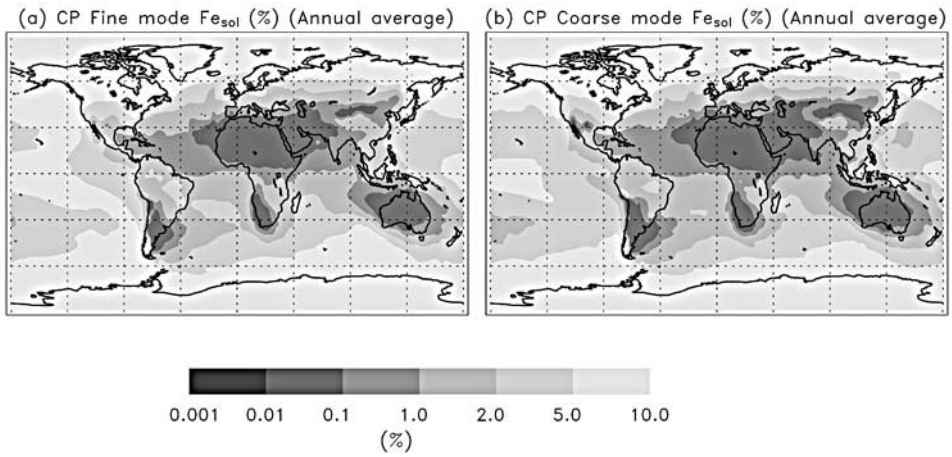

Figure 19. (a) Fine mode annually averaged (2001) global percent iron solubility (Fe_{sol}, %) estimates derived from the cloud processing case. (b) Same as Figure 19a but for the coarse particle mode.

Including the total labile Fe (Fe(II) + easily reducible Fe(III)) fraction in this definition would result in higher values of Fe_{sol} because on average (for all cruises) the fine and coarse mode Fe(II) concentrations were approximately half of total labile Fe concentrations.

[59] The estimates of percent iron solubility derived from our modeling study suggest that cloud processing and photoreduction reactions involving insoluble iron result in similar average magnitudes of soluble iron as measured during three cruises in 2001. Estimates from simple assumptions of cloud interactions were higher on average than those derived from photoreduction processes; however, these processes do not exist independently in the atmosphere. Observed percent soluble iron was higher than 40% on a few occasions; however, none of these events were reproduced by the model. It is possible that high values of iron solubility require interactions between aerosol species to assist in converting insoluble iron to a more soluble form (processes not included in the model); however, no consistent relationship between aerosol species and percent iron solubility was evident from observations.

[60] For all cruises the model was able to reproduce the observed size segregation of percent solubility, although typically exaggerating the fine mode fraction, suggesting that longer lifetimes can be responsible for the higher soluble iron fraction in the fine mode. Size selective cloud processing could also be important but was not tested with the model.

[61] The assumptions applied in this model are necessarily simple and are subject to large uncertainties. The percent solubility of iron in soils is much smaller than what is observed in atmospheric aerosols (section 3), suggesting the initial distribution of percent solubility is not that significant. Additionally, the total amount of iron in soil can vary by a factor of 2 depending on location (see Figure 11); however, once in the atmosphere these difference decrease, suggesting the variability of iron in soils is not that important (Figure 12). The largest uncertainty in modeled percent solubility therefore arises from uncertainties in modeling the total dust concentrations and in the assumptions applied in atmospheric processing. For example, we chose parameters to define cloud processing and photoreduction decay rates that are consistent with our observations; however, it is possible that other parameters better describe these processes or that our model does not do an adequate job simulating cloud events. Although the model captured the observed distribution of Fe(II) in the fine fraction, it did not capture higher observed fine mode Fe_{sol} compared to the coarse mode Fe_{sol} (Table 5). This difference may be due to the lack of size dependent processing. Selecting different *e*-folding timescales for each bin may assist in representing size selective processes. Our assumption that conversion processes are constant with height is subject to uncertainties, especially given that data on vertical distributions of clouds and dust generally are unavailable for model validation. The horizontal distribution and cloud amount in the model is also subject to uncertainty although on average the model does reproduce clouds correctly. The lack of other aerosol species in the model also contributes to uncertainties in our estimates of soluble iron. Although no clear relationship was evident from our observations, experimental studies suggest that aerosol interactions are important aspects of iron reduction processes. It is also possible that we are omitting other important aspects of these processes. For example, during the Pacific MP02 cruise, satellite observations suggested significant cloud cover, and observations demonstrated the presence of important aerosol species, yet this cruise demonstrated the lowest mean values of percent soluble iron. Clearly, we may have neglected unknown processes that may be necessary components for enhancing soluble iron. A more complex model with more aerosol species and higher resolution combined with more observations may help answer these questions. Atmospheric processing of iron in mineral aerosols is important for determining the soluble iron in deposited desert dust, especially in remote ocean regions, and requires further work. Our model results suggest that in remote regions, higher iron solubilities may enhance the ability of ocean biota to take up required iron than constant iron solubilities would suggest.

[62] **Acknowledgments.** The model simulations were done at the National Center for Atmospheric Research, which is funded by the National Science Foundation. J.L.H. would like to acknowledge Don Anderson of NASA Headquarters and the Aerocenter at the NASA Goddard Space Flight Center for supporting a visit during which the comparisons with MODIS data were performed. Dennis Savoie of University of Miami kindly provided data from Barbados. The IMPROVE data were obtained from the IMPROVE Web site (http://vista.cira.colostate.edu/improve). N.M.M., Y.C., R.S., and A.S. were supported by NSF-Biocomplexity OCE-9981398, while N.M.M. was also supported by NASA-NIP (NAG5-8680) and NASA-IDS (NAG5-9671). J.L.H. was supported by an Advanced Studies Program fellowship at NCAR. Two anonymous reviewers offered very helpful comments and suggestions.

References

Arimoto, R., R. A. Duce, B. J. Ray, and C. K. Unni (1985), Atmospheric trace elements at Enewetak atoll: Transport to the ocean by wet and dry deposition, *J. Geophys. Res.*, *90*, 2391–2408.

Arimoto, R., R. A. Duce, B. J. Ray, A. D. Hewitt, and J. Williams (1987), Trace elements in the atmosphere of American Somoa: Concentrations and deposition in the tropical South Pacific, *J. Geophys. Res.*, *92*, 8465–8479.

Arimoto, R., B. J. Ray, R. A. Duce, A. D. Hewitt, R. Boldi, and A. Hudson (1990), Concentrations, sources and fluxes of trace elements in the remote marine atmosphere of New Zealand, *J. Geophys. Res.*, *95*, 22,389–22,405.

Capone, D. G. (2001), Marine nitrogen fixation: What's the fuss?, *Current Opinion Microbiol.*, *4*(3), 341–348.

Charlson, R. J., J. E. Lovelock, M. O. Andreae, and S. G. Warren (1987), Oceanic phytoplankton, atmospheric sulphur, cloud albedo and climate, *Nature*, *326*, 655–661.

Chen, Y., and R. L. Siefert (2003), Determination of various types of labile atmospheric iron over remote oceans, *J. Geophys. Res.*, *108*(D24), 4774, doi:10.1029/2003JD003515.

Chen, Y., and R. L. Siefert (2004), Seasonal and spatial distributions and dry deposition fluxes of atmospheric total and labile iron over the tropical and subtropical North Atlantic Ocean, *J. Geophys. Res.*, *109*, D09305, doi:10.1029/2003JD003958.

Chu, D. A., Y. J. Kaufman, C. Ichoku, L. A. Remer, D. Tanré, and B. N. Holben, (2002), Validation of MODIS aerosol optical depth retrieval over land, *Geophys. Res. Lett.*, *29*(12), 8007, doi:10.1029/2001GL013205.

Claquin, T., M. Schulz, and Y. Balkanski (1999), Modeling the mineralogy of atmospheric dust sources, *J. Geophys. Res.*, *104*, 22,243–22,256.

Colin, J. L., and J. L. Jaffrezo (1990), Solubility of major species in precipitation: Factors of variation, *Atmos. Environ., Part A*, *24*, 537–544.

Cooper, D. J., A. J. Watson, and P. D. Nightingale (1996), Large decrease in ocean-surface CO_2 fugacity in response to in situ iron fertilization, *Nature*, *383*, 511–513.

Davidson, C. I., M. H. Bergin, and H. D. Kuhns (1996), The deposition of particles and gases to ice sheets, in *Chemical Exchange Between the Atmosphere and Polar Snow*, *NATO ASI Ser., Ser. I*, vol. 43, pp. 275–306, Springer-Verlag, New York.

Dubovik, O., B. N. Holben, T. Lapyonok, A. Sinyuk, M. I. Mishchenko, P. Yang, and I. Slutsker (2002), Non-spherical aerosol retrieval method

employing light scattering by spheroids, *Geophys. Res. Lett.*, *29*(10), 1415, doi:10.1029/2001GL014506.
Duce, R. A., and N. W. Tindale (1991), Atmospheric transport of iron and its deposition in the ocean, *Limnol. Oceanogr.*, *36*(8), 1715–1726.
Edwards, R., and P. Sedwick (2001), Iron in East Antarctic snow: Implications for atmospheric iron deposition and algal production in Antarctic waters, *Geophys. Res. Lett.*, *28*(20), 3907–3910.
Falkovich, A. H., E. Ganor, Z. Levin, P. Formenti, and Y. Rudich (2001), Chemical and mineralogical analysis of individual dust particles, *J. Geophys. Res.*, *106*, 18,029–18,036.
Fung, I. Y., S. K. Meyn, I. Tegen, S. C. Doney, J. G. John, and J. K. B. Bishop (2000), Iron supply and demand in the upper ocean, *Global Biogeochem. Cycles*, *14*, 281–295.
Gao, Y., S.-M. Fan, and J. L. Sarmiento (2003), Aeolian iron input to the ocean through precipitation scavenging: A modeling perspective and its implication for natural iron fertilization in the ocean, *J. Geophys. Res.*, *108*(D7), 4221, doi:10.1029/2002JD002420.
Ginoux, P., M. Chin, I. Tegen, J. M. Prospero, B. Holben, O. Dubovik, and S.-J. Lin (2001), Sources and distributions of dust aerosols simulated with the GOCART model, *J. Geophys. Res.*, *106*, 20,255–20,273.
Grini, A., and C. S. Zender (2004), Roles of saltation, sandblasting, and wind speed variability on mineral dust aerosol size distribution during the Puerto Rican Dust Experiment (PRIDE), *J. Geophys. Res.*, *109*(D7), D07202, doi:10.1029/2003JD004233.
Guelle, W., Y. J. Balkanski, M. Schulz, B. Marticorena, G. Bergametti, C. Moulin, R. Arimoto, and K. D. Perry (2000), Modeling the atmospheric distribution of mineral aerosols: Comparison with ground measurements and satellite observations for yearly and synoptic timescales over the North Atlantic, *J. Geophys. Res.*, *105*, 1997–2012.
Guieu, C., R. Chester, M. Nimmo, J.-M. Martin, S. Guerzoni, E. Nicolas, J. Mateu, and S. Keyse (1997), Atmospheric input of dissolved and particulate metals to the northwestern Mediterranean, *Deep Sea Res.*, *Part II*, *44*, 655–674.
Hack, J. (1994), Parameterization of moist convection in the NCAR community climate model (CCM2), *J. Geophys. Res.*, *99*, 5551–5568.
Hand, J. L., S. M. Kreidenweis, D. E. Sherman, J. L. Collett Jr., S. V. Hering, D. E. Day, and W. C. Malm (2002), Aerosol size distributions and visibility estimates during the Big Bend regional aerosol and visibility observational study (BRAVO), *Atmos. Environ.*, *36*, 5043–5055.
Husar, R. B., J. M. Prospero, and L. L. Stowe (1997), Characterization of tropospheric aerosols over the oceans with the NOAA advanced very high resolution radiometer optical thickness operational product, *J. Geophys. Res.*, *102*, 16,889–16,909.
Husar, R. B., et al. (2001), Asian dust events of April 1998, *J. Geophys. Res.*, *106*, 18,317–18,330.
Ichoku, C., D. A. Chu, S. Chu, Y. J. Kaufman, L. A. Remer, D. Tanré, I. Slutsker, and B. N. Holben (2002a), A spatio-temporal approach for global validation and analysis of MODIS aerosol products, *Geophys. Res. Lett.*, *29*(12), 8006, doi:10.1029/2001GL013206.
Ichoku, C., et al. (2002b), Analysis of the performance characteristics of the five-channel Microtops II Sun photometer for measuring aerosol optical thickness and precipitable water vapor, *J. Geophys. Res.*, *107*(D13), 4179, doi:10.1029/2001JD001302.
Jickells, T. D., and L. J. Spokes (2001), Atmospheric iron inputs to the ocean, in *Biogeochemistry of Iron in Seawater*, edited by D. Turner and K. A. Hunter, pp. 85–121, John Wiley, Hoboken, N. J.
Jickells, T. D., S. Dorling, W. G. Deuser, T. M. Church, R. Arimoto, and J. M. Prospero (1998), Air-borne dust fluxes to a deep water sediment trap in the Sargasso Sea, *Global Biogeochem. Cycles*, *12*, 311–320.
Johansen, A. M., R. L. Siefert, and M. R. Hoffman (1999), Chemical composition of aerosols collected over the tropical North Atlantic Ocean, *J. Geophys. Res.*, *104*, 26,325–26,347.
Johansen, A. M., R. L. Siefert, and M. R. Hoffman (2000), Chemical composition of aerosol collected over the tropical North Atlantic Ocean, *J. Geophys. Res.*, *105*, 15,277–15,312.
Kalnay, E., et al. (1996), The NCEP/NCAR 40-year reanalysis project, *Bull. Am. Meteorol. Soc.*, *77*(3), 437–471.
Kim, G., and T. Church (2001), Seasonal biogeochemical fluxes of ^{234}Th and ^{210}Po in the upper Sargasso Sea: Influence from atmospheric iron deposition, *Global Biogeochem. Cycles*, *15*, 651–661.
Kistler, R., et al. (2001), The NCEP-NCAR 50-year reanalysis: Monthly means CD-ROM and documentation, *Bull. Am. Meteorol. Soc.*, *82*(2), 247–267.
Koretsky, C., D. Sverjensky, J. Salisbury, and D. D'Aria (1997), Detection of surface hydroxyl species on quartz, gamma-alumina and feldspar using diffuse reflectance infrared spectroscopy, *Geochim. Cosmochim. Acta*, *61*(11), 2193–2210.
Lefèvre, N., and A. J. Watson (1999), Modeling the geochemical cycle of iron in the oceans and its impact on atmospheric CO_2 concentrations, *Global Biogeochem. Cycles*, *13*, 727–736.
Levy, R. C., L. A. Remer, D. Tanre, Y. J. Kaufman, C. Ichoku, B. N. Holben, J. M. Livingston, P. B. Russell, and H. Maring (2003), Evaluation of the Moderate-Resolution Imaging Spectroradiometer (MODIS) retrievals of dust aerosol over the ocean during PRIDE, *J. Geophys. Res.*, *108*(D19), 8594, doi:10.1029/2002JD002460.
Li-Jones, X., and J. M. Prospero (1998), Variations in the size distribution of non-sea-salt sulfate aerosol in the marine boundary layer at Barbados: Impact of African dust, *J. Geophys. Res.*, *103*, 16,073–16,084.
Luo, C., N. Mahowald, and J. del Corral (2003), Sensitivity study of meteorological parameters on mineral aerosol mobilization, transport and distribution, *J. Geophys. Res.*, *108*(D15), 4447, doi:10.1029/2003JD003483.
Mahowald, N. M., P. J. Rasch, B. E. Eaton, S. Whittleston, and R. G. Prinn (1997), Transport of 222 Radon to the remote troposphere using Model of Atmospheric Transport and Chemistry and assimilated winds from ECMWF and National Center for Environmental Prediction/NCAR, *J. Geophys. Res.*, *102*, 28,139–28,151.
Mahowald, N. M., C. S. Zender, C. Luo, D. Savoie, O. Torres, and J. del Corral (2002), Understanding the 30-year Barbados desert dust record, *J. Geophys. Res.*, *107*(D21), 4561, doi:10.1029/2002JD002097.
Mahowald, N., C. Luo, J. del Corral, and C. Zender (2003), Interannual variability in atmospheric mineral aerosols from a 22-year model simulation and observational data, *J. Geophys. Res.*, *108*(D12), 4352, doi:10.1029/2002JD002821.
Malm, W. C., J. F. Sisler, D. Huffman, R. A. Eldred, and T. A. Cahill (1994), Spatial and seasonal trends in particle concentration and optical extinction in the United States, *J. Geophys. Res.*, *99*, 1347–1370.
Martin, J. H., R. M. Gordon, and S. E. Fitzwater (1991), The case for iron, *Limnol. Oceanogr.*, *36*, 1793–1802.
Martins, J. V., D. Tanré, L. Remer, Y. Kaufman, S. Mattoo, and R. Levy (2002), MODIS cloud screening for remote sensing of aerosols over oceans using spatial variability, *Geophys. Res. Lett.*, *29*(12), 8009, doi:10.1029/2001GL013252.
Measures, C. I., and S. Vink (1999), Seasonal variations in the distribution of Fe and Al in the surface waters of the Arabian Sea, *Deep Sea Res.*, *Part II*, *46*, 1597–1622.
Measures, C. I., and S. Vink (2000), On the use of the dissolved aluminum in surface waters to estimate dust deposition to the ocean, *Global Biogeochem. Cycles*, *14*, 317–327.
Mishchenko, M. I., A. A. Lacis, B. E. Carlson, and L. D. Travis (1995), Nonsphericity of dust-like tropospheric aerosols: Implications for aerosol remote sensing and climate modeling, *Geophs. Res. Lett.*, *22*, 1077–1080.
Pehkonen, S. O., R. Siefert, Y. Erel, S. Webb, and M. R. Hoffman (1993), Photoreduction of iron oxyhydroxides in the presence of important atmospheric organic compounds, *Environ. Sci. Technol.*, *27*, 2056–2062.
Perry, K. D., T. A. Cahill, R. A. Eldred, and D. D. Dutcher (1997), Long-range transport of North African dust to the eastern United States, *J. Geophys. Res.*, *102*, 11,225–11,238.
Prospero, J. M. (1999), Long-term measurements of the transport of African mineral dust to the southeastern United States: Implications for regional air quality, *J. Geophys. Res.*, *104*, 15,917–15,927.
Prospero, J. M., and R. T. Nees (1986), Impact of the North African drought and El Niño on mineral dust in the Barbados trade wind, *Nature*, *320*, 735–738.
Rasch, P., and J. Kristjánsson (1998), A comparison of the CCM3 model climate using diagnosed and predicted condensate parameterizations, *J. Clim.*, *11*(7), 1587–1614.
Rasch, P. J., N. M. Mahowald, and B. E. Eaton (1997), Representations of transport, convection and the hydrologic cycle in chemical transport model: Implications for the modeling of short-lived and soluble species, *J. Geophys. Res.*, *102*, 18,127–18,138.
Remer, L. A., et al. (2002), Validation of MODIS aerosol retrieval over ocean, *Geophys. Res. Lett.*, *29*(12), 8008, doi:10.1029/2001GL013204.
Saydam, A. C., and H. Z. Senyuva (2002), Deserts: Can they be the potential suppliers of bioavailable iron?, *Geophys. Res. Lett.*, *29*(11), 1524, doi:10.1029/2001GL013562.
Seinfeld, J. H., and S. N. Pandis (1997), *Atmospheric Chemistry and Physics: From Air Pollution to Climate Change*, John Wiley, New York.
Siefert, R. L., S. O. Pehkonen, Y. Erel, and M. R. Hoffman (1994), Iron photochemistry of aqueous suspensions of ambient aerosol with added organic acids, *Geochim. Cosmochim. Acta*, *58*, 3271–3279.
Siefert, R. L., A. M. Johansen, M. R. Hoffmann, and S. O. Pehkonen (1997), Measurements of trace metal (Fe, Cu, Mn, Cr) oxidation states in fog and stratus clouds, *J. Air Waste Manage. Assoc.*, *48*, 128–143.
Siefert, R. L., A. M. Johansen, and M. R. Hoffmann (1999), Chemical characterization of ambient aerosol collected during the southwest monsoon and intermonsoon seasons over the Arabian Sea: Labile-Fe(II) and other trace metals, *J. Geophys. Res.*, *104*, 3511–3526.
Sillanpää, M. (1982), Micronutrients and the nutrient status of soils: A global study, *FAO Soils Bull. 48*, Food and Agric. Org. of the U. N.

Sokolik, I. N., and O. B. Toon (1999), Incorporation of mineralogical composition into models of the radiative properties of mineral aerosol from the UV to IR wavelengths, *J. Geophys. Res.*, *104*, 9423–9444.

Tegen, I., and I. Fung (1994), Modeling of mineral dust in the atmosphere: Sources, transport, and optical thickness, *J. Geophys. Res.*, *99*, 22,897–22,914.

Trenberth, K., and C. Guillemot (1998), Evaluation of the atmospheric moisture and hydrological process in the NCEP/NCAR reanalysis, *Clim. Dyn.*, *14*, 213–231.

Turner, S. M., P. D. Nightingale, L. J. Spokes, M. I. Liddicoat, and P. S. Liss (1996), Increased dimethyl sulphide concentrations in sea water from in situ iron enrichment, *Nature*, *383*, 513–517.

Uematsu, M., R. A. Duce, and J. M. Prospero (1985), Deposition of atmospheric mineral particles in the North Pacific Ocean, *J. Atmos. Chem.*, *3*, 123–138.

VanCuren, R. A. (2003), Asian aerosols in North America: Extracting the chemical composition and mass concentration of the Asian continental aerosol plume from long-term aerosol records in the United States, *J. Geophys. Res.*, *108*(D20), 4623, doi:10.1029/2003JD003459.

VanCuren, R. A., and T. A. Cahill (2002), Asian aerosols in North America: Frequency and concentration of fine dust, *J. Geophys. Res.*, *107*(D24), 4804, doi:10.1029/2002JD002204.

Vink, S., and C. I. Measures (2001), The role of dust deposition in determining surface water distributions of Al and Fe in the south west Atlantic, *Deep Sea Res.*, *Part II*, *48*, 2787–2809.

Warneck, P. (2003), In-cloud chemistry opens pathway to the formation of oxalic acid in the marine atmosphere, *Atmos. Environ.*, *37*, 2423–2427.

Watson, A. J., and N. Lefèvre (1999), The sensitivity of atmospheric CO_2 concentrations and input of iron to the oceans, *Tellus*, *Ser. B*, *51*, 453–460.

Watson, A. J., C. S. Law, K. A. Van Scoy, F. J. Millero, W. Yao, G. E. Friederich, M. I. Liddicoat, R. H. Wanninkhof, R. T. Barber, and K. H. Coale (1994), Minimal effect of iron fertilization on sea-surface carbon dioxide concentrations, *Nature*, *371*, 143–145.

Wolff, E. W., J. S. Hall, R. Mulvaney, E. C. Pasteur, D. Wagenbush, and M. Legrand (1998), Relationship between chemistry of air, fresh snow and firn cores for aerosol species in coastal Antarctica, *J. Geophys. Res.*, *103*, 11,057–11,070.

Zender, C. S., H. Bian, and D. Newman (2003), The Mineral Dust Entrainment And Deposition (DEAD) model: Description and 1990s dust climatology, *J. Geophys. Res.*, *108*(D14), 4416, doi:10.1029/2002JD002775.

Zhang, G., and N. McFarlan (1995), Sensitivity of climate simulations to the parameterization of cumulus convection in the Canadian climate center general circulation model, *Atmos. Ocean*, (33), 407–446.

Zhu, X., J. M. Prospero, F. J. Millero, D. L. Savoie, and G. W. Brass (1992), The solubility of ferric iron in marine mineral aerosol solutions at ambient relative humidities, *Mar. Chem.*, *38*, 91–107.

Zhu, X., J. M. Prospero, D. L. Savoie, F. J. Millero, R. G. Zika, and E. S. Saltzman (1993), Photoreduction of iron(III) in marine mineral aerosol solutions, *J. Geophys. Res.*, *98*, 9039–9046.

Zhu, X. R., J. M. Prospero, and F. J. Millero (1997), Diel variability of soluble Fe(II) and solube total Fe in North African dust in the trade winds at Barbados, *J. Geophys. Res.*, *102*, 21,297–21,305.

Zhuang, G., R. A. Duce, and D. R. Kester (1990), The dissolution of atmospheric iron in surface seawater of the open ocean, *J. Geophys. Res.*, *95*, 16,207–16,216.

Zhuang, G., Z. Yi, R. A. Duce, and P. R. Brown (1992), Link between iron and sulphur cycles suggested by detection of Fe(II) in remote marine aerosols, *Nature*, *355*, 537–539.

Zuo, Y. (1995), Kinetics of photochemical/chemical cycling of iron coupled with organic substances in cloud and fog droplets, *Geochim. Cosmochim. Acta*, *59*, 3123–3130.

Zuo, Y., and J. Hoigné (1992), Formation of hydrogen peroxide and depletion of oxalic acid in atmospheric water by photolysis of iron(III)-oxalato complexes, *Environ. Sci. Technol.*, *26*, 1014–1022.

Zwiers, F. W., and H. von Storch (1995), Taking serial correlation into account in tests of the means, *J. Clim.*, *8*, 336–351.

Y. Chen and R. L. Siefert, Chesapeake Biological Laboratory, University of Maryland Center for Environmental Science, P.O. Box 38, One Williams Street, Solomons, MD 20688, USA. (chen@cbl.umces.edu; siefert@cbl.umces.edu)

I. Fung, Department of Earth and Planetary Science, University of California, Berkeley, CA 94720, USA. (inez@atmos.berkeley.edu)

J. L. Hand, CIRA, Colorado State University, 1375 Campus Delivery, Fort Collins, CO 80523, USA. (hand@cira.colostate.edu)

C. Luo, Institute for Computational Earth System Science (ICESS), University of California, 6807 Ellison Hall, Santa Barbara, CA 93106-3060, USA. (chaoluo@bren.ucsb.edu)

N. M. Mahowald, NCAR, P.O. Box 3000, Boulder, CO 80307, USA. (mahowald@cgd.ucar.edu)

A. Subramaniam, 3 Marine Biology, Lamont-Doherty Earth Observatory of Columbia University, 61 Rt 9W, Palisades, NY 10964, USA. (ajit@ldeo.columbia.edu)